Variations and sources of volatile organic compounds (VOCs) in urban region: insights from measurements on a tall tower

Xiao-Bing Li[1,2], Bin Yuan[1,2,*], Sihang Wang[1,2], Chunlin Wang[3,4], Jing Lan[3,4], Zhijie Liu[1,2], Yongxin Song[1,2], Xianjun He[1,2], Yibo Huangfu[1,2], Chenglei Pei[5,6,7,8], Peng Cheng[9], Suxia Yang[1,2], Jipeng Qi[1,2], Caihong Wu[1,2], Shan Huang[1,2], Yingchang You[1,2], Ming Chang[1,2], Huadan Zheng[10], Wenda Yang[9], Xuemei Wang[1,2], and Min Shao[1,2]

[1] Institute for Environmental and Climate Research, Jinan University, Guangzhou 511443, China

[2] Guangdong-Hongkong-Macau Joint Laboratory of Collaborative Innovation for Environmental Quality, Guangzhou 511443, China

[3] Guangzhou Climate and Agrometeorology Center, Guangzhou, 511430, China

[4] Southern Marine Science and Engineering Guangdong Laboratory (Zhuhai), Zhuhai, 519082, China

[5] State Key Laboratory of Organic Geochemistry and Guangdong Key Laboratory of Environmental Protection and Resources Utilization, Guangzhou Institute of Geochemistry, Chinese Academy of Sciences, Guangzhou 510640, China

[6] CAS Center for Excellence in Deep Earth Science, Guangzhou, 510640, China

[7] University of Chinese Academy of Sciences, Beijing 100049, China

[8] Guangzhou Ecological and Environmental Monitoring Center of Guangdong Province, Guangzhou 510060, China

[9] Institute of Mass Spectrometer and Atmospheric Environment, Jinan University, Guangzhou 510632, Guangdong, China

[10] Guangdong Provincial Key Laboratory of Optical Fiber Sensing and Communications, and Department of Optoelectronic Engineering, Jinan University, Guangzhou, 510632, China

[*] Corresponding authors: byuan@jnu.edu.cn

Abstract

Volatile organic compounds (VOCs) are key precursors of ozone and particulate matter, which are the two dominant air pollutants in urban environments. However, compositions and sources of VOCs in urban air aloft were rarely reported so far. To address this matter, highly time-resolved measurements of VOCs were made by proton-transfer-reaction time-of-flight mass spectrometer (PTR-ToF-MS) at a 450-m platform on the Canton Tower in Guangzhou, China. A combination of *in-situ* measurements and modeling techniques was used to characterize variations and sources of VOCs. Five sources were identified from positive matrix factorization (PMF) analysis, namely daytime-mixed (e.g., biogenic emissions and secondary formation), visitor-related (e.g., human breath, cooking, and volatilization of ethanol-containing products), vehicular+industrial, regional transport, and volatile chemical product (VCP)-dominated (i.e., volatilization of personal care products), contributing on average to 21%, 30%, 28%, 10%, and 11% of total VOCs (TVOC) mixing ratios, respectively. We observe that contributions of the visitor-related source, mainly composed of ethanol, followed well with the variation in visitor numbers on the tower. The VCP-dominated source only had an average contribution of ~5.7 ppb during the campaign, accounting for a small fraction (11%) of TVOC mixing ratios but a large fraction (22%) of the total OH reactivity. However, large fractions of reactive VOC species, e.g., monoterpenes (49%), were attributed to the VCP-dominated source, indicating important contributions of VCPs to ambient concentrations of these species in urban environments. Vertical profiles of air pollutants (namely NOx, ozone, Ox, and $PM_{2.5}$), measured at 5 m, 118 m, 168 m, and 488 m, exhibited more evident gradients at night than in the daytime owing to the stronger stability of the nocturnal boundary layer. Mixing ratios of VOC species during the nighttime generally decreased with time when the 450-m platform was located in the nocturnal residual layer and markedly increased when impacted by emissions at ground. The results in this study demonstrated composition

54 characteristics and sources of VOCs in urban air aloft, which could provide valuable

55 implications in making control strategies of VOCs and secondary air pollutants.

1 Introduction

Volatile organic compounds (VOCs) are important trace gases in the atmosphere and are composed of myriad chemical species (Pallavi et al., 2019; Wang et al., 2020a; Gkatzelis et al., 2021). Except for their direct adverse impacts on human health (Zhang et al., 2013), VOCs are also important precursors of secondary pollutants such as ozone and secondary aerosol (Vo et al., 2018; Zhou et al., 2019; Qin et al., 2021). Reduction in ambient VOCs concentrations is the key for synergistic control of both ozone and particle pollution. However, it is highly challenging for this target due to complex sources and chemical transformations of VOCs in urban environments (Yuan et al., 2012; Mo et al., 2016; Zhu et al., 2019).

In addition to compiling accurate emission inventories (bottom-up method) (Zheng et al., 2013; An et al., 2021), the combination of *in-situ* measurements and receptor models (top-down method) was widely adopted to quantitatively apportion sources of ambient VOCs (Baudic et al., 2016; Liu et al., 2016; Fan et al., 2021; Pernov et al., 2021). Concentrations of various VOC species can be measured by offline and online techniques. Gas chromatography-flame ionization detector/mass spectrometry (GC-FID/MS) combined with stainless steel canisters are the most popular offline technique (Guo et al., 2011; Yuan et al., 2013; Zhang et al., 2013; Qin et al., 2021). Automated online GC-FID system and high time resolution mass spectrometer, such as proton-transfer-reaction mass spectrometer (PTR-MS) and chemical ionization mass spectrometer (CIMS), are popular online techniques (de Gouw and Warneke, 2007; Wang et al., 2020a; Wang et al., 2020c; Fan et al., 2021; Ye et al., 2021). However, VOCs measurements made by both online and offline instruments are markedly affected by very local emission sources, particularly in urban environments, when they are usually deployed at ground level. This is highly important for studies aiming to characterize variations and sources of ambient VOCs at large spatial scales (such as a city or city clusters) based on measurements of only one site. To address this concern,

83 VOCs measurements made in the upper part of the planetary boundary layer (PBL) may

84 be a better choice due to the well mixing of surface emissions when being transported

85 upward from sources to observation sites (Hu et al., 2015a; Hu et al., 2015b; Squires et

86 al., 2020).

87   As reported in the literature, *in-situ* measurements of VOCs at high altitudes (e.g.,

88 hundreds of meters or several kilometers above ground level) were predominantly made

89 using the combination of offline techniques and samples collected by various platforms

90 such as aircrafts (Geng et al., 2009; Xue et al., 2011; Benish et al., 2020), tethered

91 balloons (Zhang et al., 2018; Wu et al., 2020b; Wang et al., 2021; Wu et al., 2021), high

92 buildings and towers (Ting et al., 2008; Mo et al., 2020), and unmanned aerial vehicles

93 (UAVs) (Vo et al., 2018; Liu et al., 2021). These offline measurements were

94 predominantly used to reveal vertical variations of VOCs concentrations, impacts of

95 VOCs degradation chemistry on the formation of secondary pollutants, and source

96 characteristics of the species of interest. Offline measurements made at high altitudes

97 were generally not capable of fully characterizing temporal variations of concentrations

98 and source characteristics of VOCs due to strict limitations in their time resolution and

99 sample sizes. In this condition, online VOCs measurements with fast response at high

100 altitudes are required. Lack of available platforms has been a key limited factor for

101 conducting online VOCs measurements at high altitudes in China. For instance, the

102 combined utilization of aircraft and online spectrometer (such as PTR-MS) has been

103 widely used in North America to measure VOCs concentrations in the lower

104 troposphere (Hornbrook et al., 2011; Müller et al., 2016; Yuan et al., 2016; Koss et al.,

105 2017; Fry et al., 2018; Chen et al., 2019), while it is quite difficult in China due to the

106 lack of professional research aircraft and the strict control of airspace. Tethered balloons

107 and UAVs are generally not suitable for online VOCs measurements due to their limited

108 payloads (Dieu Hien et al., 2019). Tower-based platforms provide another path for

109 online VOCs measurements at high altitudes in urban environments. However, tower-

110 based online measurements of VOCs were only reported in Beijing, China so far

(Squires et al., 2020; Zhang et al., 2020).

In this study, continuous online VOCs measurements, including more than 200 species with a time resolution of 10 s, were made at a 450-m platform on the Canton Tower in the Pearl River Delta (PRD) region, China during August–November 2020. A combination of the VOCs measurements and the positive matrix factorization (PMF) receptor model was used to provide new insights into the concentrations, temporal variations, and source contributions of VOCs in urban region.

2 Methods and materials

2.1 Site description and field campaign

The PRD region is one of the most developed city clusters in China with more than 70 million residents by 2020 and is suffering from air pollution problems (e.g., ozone and secondary aerosol) (Wang et al., 2017; Wang et al., 2020b; Yan et al., 2020; Li et al., 2022). In this study, VOCs measurements were made at the Canton Tower (CTT, 23.11°N, 113.33°E) in Guangzhou, a large city in PRD (Figure S1), from August 18 to November 5 in 2020. The CTT has a total height of 610 m including the shaft on the top (Figure S1(c)). The observation was conducted in a room (Figure S1) at the 450-m Look Out platform (Jin et al., 2022), which is a ramp with stairs and is located on the top of the main body of the CTT. The observation room is located below the ramp and a sampling port is reserved on the wall outside the tower. A louver is located ~3 m below the sampling port. The 450-m Look Out platform is a famous tourist attraction with an opening time of local time (LT, UTC+8) 10:00–22:30, and visitors could walk around for a panorama of downtown Guangzhou. On each day, there are two busiest tourist hours, roughly at LT 11:00–14:00 and 18:00–21:00, on the 450-m platform. In addition, there are three restaurants between 376 and 423 m. The VOCs measurements were interrupted during October 8–12 due to instrument malfunction.

2.2 VOCs measurements

VOCs measurements were made using a high-resolution proton-transfer-reaction quadrupole interface time-of-flight mass spectrometer (PTR-QiToF-MS, Ionicon Analytik, Innsbruck, Austria) with both hydronium ion (H_3O^+) (Yuan et al., 2017; Wu et al., 2020a) and nitric oxide ion (NO^+) chemistry (Wang et al., 2020a). The H_3O^+ and NO^+ modes were automatically switched with 22 min for the H_3O^+ mode and 12 min for the NO^+ mode during the campaign. In this study, only VOCs measurements made in the H_3O^+ mode were used for analysis. In H_3O^+ mode, the PTR-QiToF-MS was operated with a drift tube pressure of 3.8 mbar, a drift tube temperature of 120 ℃, and a drift tube voltage of 760 V, resulting in an E/N (E refers to electric field and N refers to number density of buffer gas in the drift tube) value of ~120 Td (Townsend). Raw data of PTR-ToF-MS were processed and analyzed using Tofware software (Tofwerk AG, v3.0.3) and please refer to our previous works (Wang et al., 2020a; Wu et al., 2020a) for more details. Signals of 3035 ions with m/z up to 510 were obtained at time resolutions of 10 s. To measure VOCs concentrations outside the tower, a ~5 m long Perfluoroalkoxy (PFA) Teflon tubing (OD: 1/4") was used to connect the inlet of the instrument and the sampling port (Figure S1). The PFA Teflon tubing has been proven to be effective in measuring ambient concentrations of VOCs (Deming et al., 2019; Liu et al., 2019) and has been widely used in field studies (de Gouw et al., 2003a; Hu et al., 2011; Wu et al., 2020a). Air sample in the tubing was drawn by a pump at a flow rate of ~5 L min^{-1}. Blank measurements were performed automatically at the last 2 min of the H_3O^+ mode by passing ambient air through a platinum catalyst heated to 365 ℃.

A gas standard with 35 VOC species (Table S1) was used for calibrations of the PTR-ToF-MS once per day. Ten organic acids and nitrogen-containing VOC species were calibrated using a liquid calibration unit in the laboratory. Sensitivities of the remaining VOC species were determined using the quantification method based on reaction kinetics of the PTR-ToF-MS (Wu et al., 2020a; He et al., 2022). Impacts of the change in ambient humidity on measured signals of the PTR-ToF-MS were removed

using humidity-dependence curves of VOC species determined in the laboratory (Wang et al., 2020a; Wu et al., 2020a). The limit of detection (LOD) for a VOC species was defined as the concentration when the signal-to-noise ratio (SNR) equals to 3 (Yuan et al., 2017). Average mixing ratios, LODs, sensitivities, chemical formula, and suggested compounds of 225 VOC species used in this study are summarized in Table S1.

2.3 Other measurements

During the CTT campaign, a CO_2 and H_2O Gas Analyzer (Model: Li-840A, Licor Inc., USA) was deployed to measure carbon dioxide (CO_2, ppm in dry air) and humidity (mmol mol^{-1}). In addition, four air quality automatic monitoring stations are located at ground level (~5 m), 118 m, 168 m, and 488 m of the CTT, which report hourly concentrations of ozone, NO, NO_2, NOx, and $PM_{2.5}$ along with meteorological parameters, namely temperature (T), relatively humidity (RH), and pressure (Mo et al., 2020). Mass concentrations of gaseous pollutants were reported at 25 ℃ and 1013.25 hPa and were converted to mixing ratios (ppb) accordingly. Contour plots of vertical profiles of NOx, ozone, Ox (O_3+NO_2), and $PM_{2.5}$ concentrations were made using the bilinear method in Igor software (v8.04). Linear interpolations for concentrations of these pollutants were performed on both spatial (altitude) and temporal scales. A ceilometer (CL31, Vaisala, Finland) deployed on the Panyu Campus of Jinan University (23.02°N, 113.41°E, Figure S1), approximately 13.5 km to the southeast of the CTT, was used to measure planetary boundary layer height (PBLH) during the camapign. In addition, measurements of VOCs and CO_2 made on the campus of Guangzhou Institute of Geochemistry (GIG), Chinese Academy of Sciences (23.15°N, 113.36°E, ~25 m above ground level) during September–November 2018 (Wang et al., 2020a; Wang et al., 2020c; Wu et al., 2020a) were used for comparison with those measured on the CTT. p values were obtained using the Student's t-test to determine statistical significance levels of differences. The GIG site is located approximately 5.7 km to the northeast of the CTT. Measurements of VOCs and CO_2 at the GIG site were made using the same instruments as those at the CTT site.

2.4 PMF receptor model

The PMF receptor model was used to quantitatively analyze sources of the VOCs measurements made at the 450-m platform. The PMF model has been widely used to determine source contributions of measured VOCs concentrations in previous studies (Yuan et al., 2012; Pallavi et al., 2019; Pernov et al., 2021). A simple description of the PMF model was provided in the Supplementary Information (SI).

The PMF model was performed on 225 VOC species (Table S1) in this study. In preparation of PMF input data, measured concentrations of a VOC species below the LOD were replaced with half of the LOD and corresponding uncertainties were assigned to 5/6 of the LOD. Missing samples of a VOC species were replaced with its median value during the campaign and corresponding uncertainties were set as values equal to three times the median value (Zhang et al., 2013; Pernov et al., 2021; Qin et al., 2021). During the CTT campaign, the measured ethanol concentrations were impacted by the change in the number of visitors (a detailed discussion in Section 3.3) and exhibited strong variations (Figure 1). Thus, measurement uncertainties of ethanol calculated by Eq. (S3) were reduced by a factor of 5 to increase its weight in PMF analysis, which successfully resolved factors representing visitor influences and reduce residuals of PMF solution from over 20% to ~14%. The PMF analysis was performed using the PMF Evaluation Tool (v3.05) with Igor Pro (Ulbrich et al., 2009).

3   Results and discussion

3.1   Overview of field measurements during the campaign

As shown in Figure 1, concentrations of various species and meteorological parameters all exhibited strong variations during the campaign. Daily mean ozone mixing ratios varied in the range of 17.8–105.0 ppb with an average (± standard deviation) of 55.1 ± 18.3 ppb. Daily mean total VOCs (TVOC) mixing ratios, including a total of 225 species, varied between 23.9–124.2 ppb with an average of 62.1 ± 21.8 ppb. Daily mean NOx mixing ratios varied in the range of 7.9–31.6 ppb with an average

219   of 13.6 ± 3.8 ppb. Measured CO_2 mixing ratios exhibited strong variability with daily

220   mean values ranging from 403.5 to 471.4 ppm. Ethanol was the most abundant VOC

221   species, accounting on average for 23.5% of measured TVOC mixing ratios. Daily

222   mean ethanol mixing ratios varied between 4.3–53.4 ppb with an average of 15.3 ± 9.1

223   ppb. Toluene was the most abundant aromatic species and had an average mixing ratio

224   of 1.4 ± 0.9 ppb. Daily mean temperatures varied in the range of 17.7–29.0 °C with an

225   average of 23.2 ± 3.0 °C. Daily mean RH varied between 39.3%–85.0% with an average

226   of $71.6\% \pm 10.3\%$. In general, the observation site was predominantly influenced by

227   hot and moist air masses from August 18 to October 4, but cooler and dryer air masses

228   from October 5 to November 5.

229   The most abundant 10 VOC species measured by PTR-ToF-MS during the CTT

230   campaign were ethanol, methanol, acetic acid, formaldehyde, acetone, ethyl acetate,

231   acetaldehyde, hydroxyacetone+propionic acid, toluene, and C8 aromatics, contributing

232   to over 70% of TVOC mixing ratios. As shown in Figure 2, the 225 VOC species were

233   classified into six categories, namely C_xH_y (i.e., hydrocarbons), $C_xH_yO_1$ (i.e., VOC

234   species containing one oxygen atom), $C_xH_yO_2$ (i.e., VOC species containing two

235   oxygen atoms), $C_xH_yO_{\geq 3}$ (i.e., VOC species containing three or more oxygen atoms),

236   N/S containing species (i.e., VOC species containing nitrogen or sulfur atoms), and

237   siloxanes (Wu et al., 2020a; He et al., 2022). The most abundant category was $C_xH_yO_1$,

238   which had an average contribution of 67% to TVOC mixing ratios, but only contributed

239   to 40% of total OH reactivity. The $C_xH_yO_2$ and $C_xH_yO_{\geq 3}$ categories contributed to 22%

240   and 1% of TVOC mixing ratios, respectively. C_xH_y only accounted for 9% of TVOC

241   mixing ratios but contributed to 37% of the total OH reactivity, indicating more reactive

242   VOC species in this category. Concentrations of N/S containing species and siloxanes

243   were generally lower than 0.5 ppb and totally contributed to ~1% of TVOC mixing

244   ratios.

245   At ground level, each VOCs category accounted for comparable fractions in

246   TVOC mixing ratios and the total OH reactivity to those measured at 450 m. However,

247   the majority of the C_xH_y, $C_xH_yO_{\geq 3}$, and N/S containing species measured at 450 m had

248   lower mixing ratios than those measured at ground level (Figures 2(b) and S2),

249   implying their predominant contributions from surface emission sources. Most of the

250    $C_xH_yO_1$ and $C_xH_yO_2$ species measured at 450 m had comparable mixing ratios to those

251   measured at the ground level. However, mixing ratios of some $C_xH_yO_2$, $C_xH_yO_{\geq 3}$, and

252   N/S containing species measured at 450 m were higher than those measured at ground

253   level, which can be attributable to either enhancement of their emissions on the 450-m

254   platform or more secondary formation from oxidation of VOCs (e.g., C_xH_y and $C_xH_yO_1$

255   species). The differences in contributions of VOCs categories to the total concentrations

256   and OH reactivity imply that sources of the VOCs measurements made at 450 m and

257   the ground level are different.

3.2   Diurnal variations in selected VOC species

259   Average diurnal profiles of nine selected VOC species measured by PTR-ToF-MS

260   during the CTT campaign are demonstrated in Figure 3. Measurement results at GIG in

261   2018 are also shown for comparison to investigate differences in their diurnal variation

262   patterns and likely sources. In addition, average diurnal profiles of the selected VOC

263   species on working and non-working days (including weekends and public holidays

264   when the 450-m platform had more visitors) during the CTT campaign are compared

265   to explore potential emissions from visitors. Average diurnal variations in ratios of

266   concentrations of selected VOC species measured on non-working days to those

267   measured on working days were also calculated, as shown in Figure S3. Meteorological

268   factors, namely temperature and RH, exhibited insignificant differences between

269   working and non-working days (Figure S4). Thus, the differences in VOCs

270   concentrations between working and non-working days were not notably impacted by

271   the change in meteorological conditions.

272   Diurnal profiles of aromatic species, including benzene, toluene, and C8 aromatics

273   measured at 450 m exhibited similar variability with minima occurring between LT

274   12:00–16:00. Aromatics with higher chemical reactivity could be removed more rapidly

275 by reactions with hydroxyl radicals (OH) in the daytime (Yuan et al., 2012; Wu et al.,

276 2020a). In addition, rapid elevation of the daytime PBL could enhance the dilution of

277 chemical species, leading to rapid decreases in their concentrations (Sangiorgi et al.,

278 2011; Zhang et al., 2018). The two effects are the two most important factors for

279 controlling diurnal profiles of aromatics measured at 450 m. By contrast, diurnal

280 profiles of aromatics measured at ground displayed a different pattern with two peaks

281 occurring in the morning (LT 07:00–08:00) and evening (LT 19:00–22:00), respectively.

282 Diurnal patterns of aromatics are consistent with that of NOx (a typical tracer of traffic

283 emissions in urban region) at ground level but were different from that of NOx at 450

284 m (Figure 4). Therefore, measured concentrations of aromatics, particularly for benzene,

285 were markedly affected by traffic emissions at ground level, but contributed by more

286 complex sources at 450 m. The differences in diurnal profiles of aromatics between

287 working and non-working days were insignificant ($p>0.05$), implying minor

288 contributions from visitor-related emissions. On working days, toluene concentrations

289 measured at 450 m were more affected by traffic emissions as manifested by the two

290 remarkable peaks in the morning and late afternoon.

291   Isoprene and monoterpenes exhibited distinct diurnal variation patterns during the

292 two campaigns. As reported in (Gómez et al., 2020; Tan et al., 2021), diurnal profiles

293 of isoprene and monoterpenes concentrations in non-urban regions usually displayed

294 unimodal patterns with a peak occurring at noon due to the strong light/temperature-

295 dependence of biogenic emissions. In this study, isoprene concentrations at 450 m

296 plateaued during the daytime and were slightly higher on non-working days than those

297 on working days, implying large contributions from visitor-related emissions. The

298 diurnal profile of monoterpenes measured at 450 m exhibited a bimodal pattern with

299 two peaks at LT 14:00 and 20:00, which was roughly in accordance with diurnal peaks

300 of visitor numbers on the 450-m platform. In addition, monoterpenes concentrations at

301 450 m were significantly ($p<0.01$) higher on non-working days (particularly during the

302 busiest tourist hours) than on working days, confirming significant contributions from

303   visitor-related or cooking emissions (Klein et al., 2016). The diurnal profiles of methyl

304   vinyl ketone (MVK) + methacrolein (MACR) demonstrated similar shapes to ozone at

305   both 450 m and ground level with maxima occurring between LT 13:00–15:00 (Figure

306   4), consistent with MVK+MACR as photooxidation products of isoprene (Greenberg

307   et al., 1999; Zhao et al., 2021). The concentrations of MVK+MACR during the daytime

308   on non-working days were also significantly ($p<0.01$) higher than those on working

309   days, which are consistent with isoprene observations.

310   Acetone, methanol, and ethanol are abundant OVOC species in urban atmosphere.

311   Diurnal profiles of acetone measured at both 450 m and the ground level were

312   characterized by higher concentrations in the daytime, suggesting predominant

313   contributions from daytime sources, such as vegetation emissions and photooxidation

314   of hydrocarbons (Hu et al., 2013; Gkatzelis et al., 2021). In addition, acetone

315   concentrations at 450 m were higher on non-working days than on working days,

316   implying prominent contributions from visitor-related emissions. Diurnal profiles of

317   methanol and ethanol measured at ground level were characterized by a bimodal pattern

318   with two peaks occurring in the morning (LT 08:00) and evening (LT 20:00),

319   respectively, confirming strong contributions from traffic emissions. However,

320   methanol concentrations measured at 450 m exhibited weak diurnal variability and

321   lower concentrations on non-working days, indicating that they were less affected by

322   visitor-related emissions. The diurnal profile of ethanol at 450 m displayed two peaks

323   at LT 13:00 and 19:00, respectively, which was in accordance with the two busiest

324   tourist hours of the 450-m platform. In addition, ethanol concentrations at 450 m on

325   non-working days were significantly ($p<0.01$) higher than those on working days,

326   particularly in the opening hours of the 450-m platform. These results suggest that the

327   ethanol concentrations measured at 450 m were largely contributed by visitor-related

328   emissions.

329   To further explore spatial scales of emission source regions for different VOC

330   species, autocorrelation profiles of their time series were calculated by offsetting time

from -120 to 120 min. As indicated in previous studies (Hayes et al., 2013; Hu et al., 2016), concentrations of a species that is more affected by local sources would have a narrower autocorrelation profile. As shown in Figure 4, peak widths of autocorrelation profiles for different species at 450 m strongly varied. Autocorrelation profiles of monoterpenes, toluene, ethanol, methanol, and isoprene were relatively narrower (even narrower than the autocorrelation profile of NOx), and thus sources of these species had more local characteristics. Autocorrelation profiles of benzene, C8 aromatics, acetone, and MVK+MACR were much flatter (but narrower than the autocorrelation profile of ozone and Ox), indicating that concentrations of these species were more contributed by sources at larger spatial scales. By contrast, peak widths of the autocorrelation profiles for different species (except for ethanol) were comparable to that of NOx. Therefore, concentrations of the selected VOC species were notably contributed by local traffic emissions at ground level but contributed by more complex sources on larger spatial scales at 450 m.

3.3 Impacts of visitor-related emissions on VOCs measurements

As introduced in section 2.1, the CTT campaign was conducted in August-November of 2020, during which visitors were required to wear masks when visiting the CTT and ethanol-containing products were widely used to prevent the spread of the COVID-19 pandemic. For example, medicinal alcohol (75%) spray was widely used to wipe public utilities and 75%-ethanol bacteriostatic gel was extensively used as sanitizer for hands. The total usage of ethanol-containing products was closely associated with the number of visitors. This can be manifested by the diurnal profiles of some VOC species (e.g., ethanol) that exhibited similar variation patterns to that of the number of visitors at the 450-m platform, as shown in Figure 3. In addition, the restaurants are located ~30 m below the observation site and emission intensities of VOCs (e.g., monoterpenes) from cooking-related sources were also closely associated with the number of visitors. Therefore, the VOCs measurements were inevitably affected by visitor-related emissions, such as human breath, cooking, and volatilization

359 of ethanol-containing and personal care products (Veres et al., 2013).

360   As shown in Figure 5(a), the diurnal profile of CO_2 measured at 450 m increased

361 between LT 09:00–20:00, which was different from those measured at ground level.

362 The higher CO_2 mixing ratios at 450 m were predominantly contributed by human

363 breath due to the absence of combustion sources. Measured ethanol mixing ratios were

364 well correlated with those of CO_2 (R^2=0.36, p<0.01) during the CTT campaign (Figure

365 5(b)), indicating that ethanol concentrations, as well as its variations, were

366 predominantly determined by the change in the number of visitors on the tower. In

367 addition, the CO_2 mixing ratios on non-working days, especially during the busiest

368 tourist hours, were significantly (p<0.01) higher than those on working days. The 450-

369 m platform was closed during October 13-15 as the result of the influence of Typhoon

370 Kompasu. On these days, mixing ratios of ethanol, CO_2, and monoterpenes exhibited

371 similar variation patterns to benzene (a typical tracer of traffic emissions), as shown in

372 Figure 5(c). However, mixing ratios of ethanol, CO_2, and monoterpenes exhibited quite

373 different variation patterns from benzene when the 450-m platform was re-open

374 (October 16–21). For instance, mixing ratios of ethanol, CO_2, and monoterpenes

375 generally decreased from LT 12:00 to 18:00 between October 13–15, but markedly

376 increased during the same period between October 16–21. Therefore, it can be

377 concluded that the VOCs measurements made at 450 m were significantly affected by

378 visitor-related emissions, which will be quantitatively assessed using the PMF analysis

379 in following sections.

380 **3.4 Source analysis of VOCs measurements**

381   In this study, a five-factor solution for the PMF analysis was chosen as the optimal

382 result. Figure 6 displays source profiles (m/z ≤ 150, the full range of the mass spectra

383 is shown in Figure S7) of the five PMF factors along with average diurnal profiles of

384 their contributions. The five factors were assigned to likely sources of daytime-mixed,

385 visitor-related, vehicular+industrial, regional transport, and volatile chemical product

386 (VCP)-dominated according to characteristics of their source profiles and temporal

387   variations, which are detailedly discussed in the *SI*.

388   The visitor-related source predominantly includes contributions from human

389   breath and volatilization of ethanol-containing and personal care products.

390   Contributions of the visitor-related source had the narrowest autocorrelation profile

391   among the five factors (Figure 6(g)), confirming its most local characteristics. As shown

392   in Figure 7, the visitor-related source had the largest contributions (15.9 ± 19.6 ppb),

393   accounting for 30% of the average TVOC mixing ratio. In addition, contributions of the

394   visitor-related source accounted for a larger fraction of TVOC mixing ratios on non-

395   working days (33%) than those on working days (28%), as shown in Figures 7 and S8.

396   It should be noted that visitor-related emissions belonged to highly local sources on the

397   450 m platform and were not typical of the VOCs measurements in the upper boundary

398   layer. The vehicular+industrial source mainly includes contributions from vehicular

399   exhausts and emissions of various industrial processes. Contributions of the

400   vehicular+industrial source (15.1 ± 18.3 ppb) were comparable to those of the visitor-

401   related source, accounting for 28% of the average TVOC mixing ratio. As anticipated,

402   the vehicular+industrial source contributed to a smaller fraction of TVOC mixing ratios

403   on non-working days (26%) than those on working days (30%). The VCP-dominated

404   source predominantly includes contributions from the volatilization of VCPs in urban

405   environments. The VCP-dominated source had an average contribution of 5.7 ± 5.4 ppb,

406   accounting for 11% of the average TVOC mixing ratio. The average contribution of the

407   VCP-dominated source in this study was comparable to those (~6.0 ppb) measured in

408   New York City (Gkatzelis et al., 2021). However, VCPs contributed to over 50% of

409   anthropogenic VOCs emissions in New York City, which is much greater than the

410   fraction in this study (11%, and it will increase to 16% when contributions of the visitor-

411   related source were removed). In comparison to large cities in U.S., traffic and

412   industrial emissions were still dominant sources of ambient VOCs in Chinese cities.

413   However, VCPs emissions should also be given more attention as the VCP-dominated

414   (22%) and vehicular+industrial (23%) sources had comparable contributions to the total

415   OH reactivities, as shown in Figure 7(f).

416   The daytime-mixed source predominantly includes contributions from biogenic

417   emissions and photooxidation products of various VOCs. The daytime-mixed source

418   had an average contribution of 11.6 ± 12.6 ppb, accounting for 21% of the average

419   TVOC mixing ratio. It exhibited consistent diurnal variation patterns on both working

420   and non-working days but had larger contributions in the daytime on non-working days

421   (Figure 6). This may be attributed to the enhanced formation of secondary OVOC

422   species as manifested by the higher ozone concentrations on non-working days (Figure

423   S9). The regional transport source mainly includes contributions from advection

424   transport of aged air masses. Contributions of the regional transport source had the

425   flattest autocorrelation profile, implying its most regional characteristics. Only a small

426   fraction (<5%) of reactive chemical species such as aromatics were attributed to this

427   factor, leading to the lowest contribution to the total OH reactivity. Contributions of the

428   regional transport source accounted for 13% of the TVOC mixing ratio when affected

429   by continental airflows, but only accounted for 3% when affected by marine airflows

430   (Figure S10). By contrast, contributions of the other factors displayed weak

431   dependences on wind direction.

432   As shown in Figure 8, source apportionment of the selected VOC species (Figure

433   3) discussed in section 3.2 were further investigated. The vehicular+industrial source

434   had the largest contribution (36%) to benzene. The daytime-mixed source also

435   contributed to 18% of measured benzene mixing ratios. In addition, more than 20% of

436   benzene was attributed to the VCP-dominated source. In contrast to benzene, toluene

437   was predominantly attributed to the vehicular+industrial (93%) and visitor-related (7%)

438   sources. The average ratio of toluene to benzene was 5.7 ppb/ppb during the CTT

439   campaign (Figure S11), further confirming primary contributions of toluene from

440   vehicular and industrial emissions (Wu et al., 2016; Zhou et al., 2019; Xia et al., 2021).

441   The vehicular+industrial source also accounted for the largest fractions of C8 and C9

442   aromatics. In addition, 26% of C8 aromatics and 38% of C9 aromatics were attributed

to the VCP-dominated source. The other three sources in total contributed to less than 10% of concentrations of C8 and C9 aromatics. These results indicate that VCPs are important sources of aromatics in urban environments but they were rarely identified in previous studies.

Isoprene and monoterpenes are widely known tracers of biogenic emissions (Millet et al., 2016; Zhao et al., 2021). However, the daytime-mixed source only contributed to 16% of measured isoprene mixing ratios. By contrast, more than 70% of isoprene were attributed to the visitor-related (38%) and VCP-dominated (35%) sources. As for monoterpenes, more than 95% of the measured mixing ratios were attributed to the visitor-related (47%) and VCP-dominated (49%) sources. The average ratio of monoterpene to isoprene mixing ratios at 450 m was 0.84 in the daytime (LT 08:00–18:00), which was significantly ($p<0.01$) greater than that at the ground level (0.05) (Figure S11). It further confirms strong contributions of monoterpenes from visitor-related emissions at the 450-m platform. The daytime-mixed source did not exhibit discernible contributions to monoterpenes. This agrees well with the results in New York City where monoterpene mixing ratios were primarily attributed to anthropogenic sources such as VCPs, cooking, and building materials (Coggon et al., 2021; Gkatzelis et al., 2021). These results suggest that emission intensities of isoprene and monoterpenes may be highly underestimated in urban regions if their anthropogenic emissions are overlooked or less considered. This is exceedingly important for air quality models when estimating formation of ozone and secondary organic aerosol driven by the oxidation of isoprene and monoterpene. As the key photooxidation products of isoprene, nearly 60% of MVK+MACR were attributed to the daytime-mixed source. The visitor-related, regional transport, and VCP-dominated sources contributed to comparable fractions (11%–15%) of MVK+MACR. Therefore, anthropogenic emissions are also important sources of MVK+MACR in urban environments.

As shown in Figure 8, 39% of acetone was attributed to the daytime-mixed source.

The vehicular+industrial (19%) and VCP-dominated (21%) sources accounted for comparable fractions of measured acetone mixing ratios. The visitor-related source had the lowest contribution (7%) to acetone. As for methanol, the vehicular+industrial source accounted for the largest fraction (38%), followed by the daytime-mixed (22%), regional transport (17%), VCP-dominated (14%), and visitor-related (9%) sources. These results reveal that VCPs also contributed significantly to ambient concentrations of acetone and methanol and should be carefully considered when estimating their total emission intensities from anthropogenic sources. Ethanol was predominantly attributed to the visitor-related source. Therefore, the enhanced ethanol mixing ratios were not capable of representing its characteristic concentrations in urban environments. Although the absence of synchronous ground-level measurements, we can speculate that ethanol concentrations at ground level were also increased during the outbreak of the COVID-19 pandemic due to the extensive usage of ethanol-containing products. The enhancement of ethanol concentrations can contribute significantly to the increase in atmospheric OH reactivity (Millet et al., 2012; de Gouw et al., 2017; de Gouw et al., 2018) and then regulate the formation of secondary pollutants. Therefore, impacts of the ethanol enhancement on ambient air quality should be explicitly investigated in future studies due to the wide report of ozone enhancement during the outbreak of the COVID-19 pandemic (Huang et al., 2020; Qi et al., 2021).

Acetonitrile is widely used as a typical tracer of biomass burning sources in previous studies (de Gouw et al., 2003b; Zhang et al., 2020; Tan et al., 2021). However, biomass burning source was not identified in this study because acetonitrile was not predominantly attributed to a single factor. In addition to the visitor-related source, the other four sources also had large contributions to acetonitrile. As indicated by (Huangfu et al., 2021), it is not always suitable, particularly in urban environments, to use absolute concentrations of acetonitrile as the indication of biomass burning sources. The ratio of acetonitrile to CO is a better indicator to identify whether VOCs measurements are predominantly contributed by biomass burning emissions. The average ratio of

499   acetonitrile to CO was only 0.09 (ppb ppm^{-1}) during the CTT campaign (Figure S11),

500   indicating negligible contributions from biomass burning sources. In addition to the

501   daytime-mixed (22%) and vehicular+industrial (26%) sources, the VCP-dominated

502   source (31%) also had large contributions to acetonitrile in urban environments.

503   **3.5   Vertical distributions of air pollutants concentrations**

504   As introduced in section 2.1, hourly concentrations of some air pollutants were

505   routinely measured at four automatic sites on the CTT. Figure 9 shows contour plots of

506   vertical profiles of NOx, ozone, Ox (O$_3$+NO$_2$), and PM$_{2.5}$ concentrations in September

507   2020. Concentrations of the four pollutants all exhibited stratified structures between

508   488 m and the ground level. Higher mixing ratios of ozone and Ox predominantly

509   occurred at higher altitudes, while higher NOx mixing ratios mainly occurred at ground

510   level. By contrast, higher PM$_{2.5}$ concentrations were observed at both middle altitudes

511   and ground level.

512   To further clarify vertical distribution patterns of air pollutants concentrations,

513   their composite profiles for daytime (LT 08:00–18:00), nighttime (LT 19:00–05:00),

514   and the whole day in the campaign were determined, respectively, as shown in Figure

515   10. Vertical profiles of air pollutant concentrations exhibited similar shapes both in

516   daytime and nighttime. NOx mixing ratios decreased from the ground level to 488 m,

517   suggesting intensive surface emissions around the CTT. Ozone mixing ratios rapidly

518   increased from the ground level to 488 m, which was consistent with the results reported

519   in previous studies (Velasco et al., 2008; Li et al., 2018; Zhang et al., 2019; Li et al.,

520   2021b). The positive gradients of ozone profiles are mainly caused by enhanced NO

521   titration (NO+O$_3$=O$_2$+NO$_2$) and dry deposition near ground. Ox mixing ratios also

522   increased from the ground level to 488 m but exhibited weaker gradients in comparison

523   to ozone. Vertical profiles of PM$_{2.5}$ concentrations exhibited similar shapes to NOx.

524   Daily mean concentrations of PM$_{2.5}$ and Ox were well correlated at the four altitudes

525   with r values varying in the range of 0.61–0.82, suggesting prominent contributions of

526   secondary formation to ambient PM concentrations. Moreover, the correlation

527 coefficients between Ox and PM$_{2.5}$ concentrations at 488 m (0.82) were greater than

528 those at ground level (0.78), as they were less affected by nearby vehicular emissions.

529 This is consistent with the work by (Yan et al., 2020), who reported that secondary

530 components contributed to ~80% of PM$_{2.5}$ concentrations in PRD over the 2008–2019

531 period.

532 As shown in Figures 9 and 10, vertical profiles of air pollutant concentrations

533 exhibited weaker gradients in the daytime than in the nighttime. Therefore, the daytime

534 VOCs chemistry may have minor differences between the ground level and the 450-m

535 site due to strong vertical mixing of chemical species in the planetary boundary layer

536 (PBLH>450 m, as shown in Figure S12). In the nighttime, the oxidative products (such

537 as organic nitrates and OVOCs) of unsaturated hydrocarbons, predominantly initiated

538 by nitrate radicals (NO$_3$) and ozone, are also important precursors of secondary aerosol

539 (Warneke et al., 2004; Brown et al., 2011; Ng et al., 2017; Liebmann et al., 2019).

540 However, it is highly challenging to investigate the nighttime VOCs chemistry with

541 only ground-level measurements due to the rapid removal of NO$_3$ radicals and ozone

542 by enhanced NO titration (Geyer and Stutz, 2004; Stutz et al., 2004; Brown et al., 2007).

543 In this condition, the nocturnal residual layer, separated from nocturnal boundary layer

544 and remained, to a large extent, the chemical composition of the daytime atmosphere,

545 could provide an ideal place for investigating nighttime VOCs chemistry. Oxidative

546 products of VOCs in the residual layer could be mixed downward with the expansion

547 of the PBL during the daytime (Geyer and Stutz, 2004; Stutz et al., 2004; Li et al.,

548 2021a), contributing to the formation of ozone and secondary aerosol at ground level.

549 Investigation of the nighttime VOCs chemistry was one of the initial purposes of this

550 study. Unfortunately, the 450-m site was rarely located in the nocturnal residual layer

551 during the CTT campaign due to frequent occurrences of cloudy and rainy weather. The

552 average nighttime PBLH in Guangzhou was approximately stabilized at 500 m during

553 the campaign (Figure S12), implying notable impacts from surface emissions on the

554 measurements made at 450 m.

555   In addition to the measured PBLH data, formation of the residual layer at 450 m

556   could be also identified by comparing differences of ozone mixing ratios between 488

557   m and the ground level. Without fresh NO emissions, ozone mixing ratios in the

558   nocturnal residual layer were markedly higher than at ground level and exhibited weak

559   variability throughout the nighttime (Caputi et al., 2019; Udina et al., 2020). By contrast,

560   surface ozone mixing ratios are generally very low (close to zero) due to enhanced

561   titration by freshly emitted NO and strong inhibition of atmospheric vertical mixing

562   (Ma et al., 2011; Chen et al., 2020). In this study, the data collected between September

563   27–30 was one of the cases discussed above and was used to briefly describe behaviors

564   of some representative VOC species (namely ethanol, monoterpene, styrene, phenol,

565   and toluene) at 450 m.

566   As shown in Figure 11, ozone mixing ratios measured at ground level (10.2 ± 10.4

567   ppb) were significantly ($p<0.01$) lower than those at 488 m (44.2 ± 19.6 ppb) on the

568   nighttime of September 27–30, indicating formation of the nocturnal residual layer

569   lower than 450 m. On the nighttime of September 27–28, ozone mixing ratios at 488 m

570   slightly fluctuated around 46.8 ppb between LT 19:00–00:00 and suddenly decreased

571   to 28.4 ppb at LT 01:00 on September 28. The sudden decrease in ozone at LT 01:00

572   was accompanied by slight increases in both NOx and VOCs but notable decreases in

573   NOx and NO at ground level, indicating a transitory intrusion of surface fresh emissions

574   into the residual layer. On September 28, ozone mixing ratios at 488 m slightly

575   decreased from 33.0 to 31.5 ppb from LT 02:00 to 05:00, during which mixing ratios

576   of NOx and VOCs all decreased in different degrees. The continuous decreases in both

577   toluene and ethanol between LT 02:00–05:00 confirm that the VOCs measurements at

578   450 m were free of interferences by fresh emissions due to their large contributions

579   from vehicular exhausts (Figure 8). Toluene mixing ratios decreased by 43% from LT

580   02:00 to 05:00, which was larger than those (12–27%) of the other VOC species shown

581   in Figure 11. However, the NO₃ reactivity (characterized by reaction rate constants of

582   VOC species to NO₃ radical, k_{NO3}) of toluene ($k_{NO3} = 7\times10^{-17}$ cm^3 molecule^{-1} s^{-1}) is

583   exceedingly lower than those of the other unsaturated VOC species (k_{NO3} varies in the

584   magnitudes of 10^{-12} cm^3 $molecule^{-1}$ s^{-1}) (Atkinson and Arey, 2003; Atkinson et al.,

585   2006). Therefore, the decline of unsaturated VOC species in the nocturnal residual layer

586   may not be all attributed to the degradation chemistry initiated by NO_3 radicals or ozone.

587   On the nighttime of September 28–29, the PBLH was higher than 500 m between

588   LT 19:00–00:00, resulting in notable decreases in ozone and increases in NOx and

589   VOCs. As shown in Figure 11, the 450-m site may locate in the residual layer after LT

590   01:00. However, the rapid decrease in mixing ratios of NOx and VOCs between LT

591   01:00–05:00 were not likely caused by chemical removal due to the rapid increase in

592   ozone. Regional transport of aged air masses (characterized by high ozone and low NOx

593   mixing ratios) may be responsible for the rapid decline in various VOC species in the

594   early morning of September 29. On the nighttime of September 29–30, the 450-m site

595   may be impacted by surface fresh emissions as mixing ratios of ozone, NOx, and VOCs

596   all decreased between LT 19:00–01:00 and simultaneously increased between LT

597   02:00–05:00. NOx and toluene mixing ratios generally increased between LT 12:00–

598   18:00 during September 27–29, which were quite different from their average diurnal

599   variation patterns during the whole campaign (Figures 3 and 4). As discussed above,

600   the 450-m site was located in the nocturnal residual layer during September 27–29.

601   Therefore, emissions of pollutants from surface sources could be mixed upward to the

602   measurement site only when the PBLH was higher than 450 m. Furthermore, the PBL

603   was relatively lower and rapidly shrank in the afternoon, leading to the accumulation

604   of chemical species at 450 m.

605   In summary, the VOCs measurements made by PTR-ToF-MS at the 450-m site

606   can be used to characterize variations in VOC species from their primary emissions

607   during the nighttime. Nevertheless, the oxidative degradation processes of VOCs in the

608   nighttime were not well captured. It is highly difficult to provide more information on

609   the nighttime chemistry of VOC species solely depending on their temporal variations.

610   We believe that the oxidative degradation of reactive VOC species did occur in the

611 nocturnal residual layer due to the coexistence of high concentrations of NOx and ozone.

612 Measurement techniques that targeting oxidation products (e.g., ToF-CIMS) and

613 numerical models should be jointly used to deeply analyze the nighttime chemistry of

614 VOCs in the nocturnal residual layer and quantitatively evaluate their impacts on

615 ambient air quality during the daytime.

4   Conclusions

617   Continuous measurements of VOCs mixing ratios were made by PTR-ToF-MS at

618 450 m on the CTT in PRD, China from August 18–November 5, 2020. In addition to

619 some specific VOC species (such as ethanol and monoterpenes) that were intensively

620 emitted by visitor-related sources, mixing ratios of most VOC species at 450 m were

621 generally lower than those at ground level. Due to intensive emissions from visitor-

622 related sources, mixing ratios of some VOC species were significantly higher on non-

623 working days than those on working days. The VOCs mixing ratios measured at 450 m

624 also exhibited different diurnal variations from those at ground level, indicating that

625 they were contributed by more mixed sources at larger spatial scales. Five sources,

626 namely daytime-mixed, visitor-related, vehicular+industrial, regional transport, and

627 VCP-dominated, were determined by the PMF model, contributing to 21%, 30%, 28%,

628 10%, and 11% of the average TVOC mixing ratio, respectively. In addition to the

629 daytime-mixed and visitor-related sources, the other three sources all had relatively

630 lower contributions on non-working days than on working days. The VCP-dominated

631 source contributed an average of 5.7 ppb to TVOC mixing ratios, which was

632 comparable to those reported in American cities (Gkatzelis et al., 2021). However, the

633 VCP-dominated source accounted for a much smaller fraction (11%) of measured

634 TVOC mixing ratios in this study than in U.S. cities (>50%). Therefore, the reduction

635 in anthropogenic VOC emissions from traffic and industrial sources are still priorities

636 of current air pollution control for Chinese cities. Though smaller fraction of VOCs

637 contributed by VCPs was observed in this study compared to cities in U.S. (McDonald

638 et al., 2018; Gkatzelis et al., 2021), large fractions of key VOC species (such as
639 monoterpenes and some aromatic species) were attributed to the VCP-dominated
640 source. In addition, the VCP-dominated (22%) and vehicular+industrial sources (23%)
641 had comparable contributions to the total OH reactivity. Therefore, VCPs emissions
642 should be given more attentions when making control strategies for VOCs in urban
643 region..

644 The vertical distribution patterns of NOx, ozone, Ox, and PM$_{2.5}$ concentrations
645 were investigated using measurements made at four different heights on the CTT.
646 Vertical profiles of NOx and PM$_{2.5}$ generally exhibited negative gradients, while
647 vertical profiles of ozone demonstrated positive gradients. In addition, the vertical
648 gradients of air pollutant concentrations were larger in the nighttime than in the daytime,
649 predominantly owing to stronger stability of the nocturnal boundary layer. The 450-m
650 site was rarely located in the nocturnal residual layer as cloudy and rainy weather
651 dominated during the campaign. The selected case revealed that the NO$_3$- or O$_3$-
652 initiated degradation chemistry may be not the sole path for the removal of unsaturated
653 VOC species in nighttime. The degradation chemistry of reactive VOC species in the
654 nocturnal residual layer and their impacts on ground-level air quality could be further
655 investigated in combination with model simulations in future studies.

Data availability

657 The observational data used in this study are available from corresponding authors
658 upon request.

Author contributions

660 XBL and BY designed the research. XBL, BY, SHW, CLW, JL, ZJL, XJH, YBHF,
661 CLP, CP, JPQ, CHW, YCY, MC, HDZ, WDY, XMW, and MS contributed to the data
662 collection and data analysis. XBL and BY performed the PMF analysis with
663 contributions from YXS, SXY, and SH. XBL and BY wrote the paper. All the coauthors

664   discussed the results and reviewed the paper.

Competing interests

666   The authors declare that they have no conflict of interest.

Acknowledgments

668   This work was financially supported by the National Key R&D Plan of China (grant

669   No. 2019YFE0106300), Guangdong Natural Science Funds for Distinguished Young

670   Scholar (grant No. 2018B030306037), the National Natural Science Foundation of

671   China (grant No. 41877302, 42121004), Key-Area Research and Development

672   Program of Guangdong Province (grant No. 2020B1111360003), China Postdoctoral

673   Science Foundation (grant No. 2019M663367), Guangdong Innovative and

674   Entrepreneurial Research Team Program (grant No. 2016ZT06N263), and Special Fund

675   Project for Science and Technology Innovation Strategy of Guangdong Province (grant

676   No. 2019B121205004). We sincerely appreciate the help and support from the Canton

677   Tower Management Team.

References

An, J., Huang, Y., Huang, C., Wang, X., Yan, R., Wang, Q., Wang, H., Jing, S., Zhang, Y., Liu, Y., Chen, Y., Xu, C., Qiao, L., Zhou, M., Zhu, S., Hu, Q., Lu, J., and Chen, C.: Emission inventory of air pollutants and chemical speciation for specific anthropogenic sources based on local measurements in the Yangtze River Delta region, China, Atmos. Chem. Phys., 21, 2003-2025, https://doi.org/10.5194/acp-21-2003-2021, 2021.

Atkinson, R., and Arey, J.: Atmospheric Degradation of Volatile Organic Compounds, Chem Rev, 103, 4605-4638, https://doi.org/10.1021/cr0206420, 2003.

Atkinson, R., Baulch, D. L., Cox, R. A., Crowley, J. N., Hampson, R. F., Hynes, R. G., Jenkin, M. E., Rossi, M. J., Troe, J., and Subcommittee, I.: Evaluated kinetic and photochemical data for atmospheric chemistry: Volume II – gas phase reactions of organic species, Atmos. Chem. Phys., 6, 3625-4055, https://doi.org/10.5194/acp-6-3625-2006, 2006.

Baudic, A., Gros, V., Sauvage, S., Locoge, N., Sanchez, O., Sarda-Estève, R., Kalogridis, C., Petit, J. E., Bonnaire, N., Baisnée, D., Favez, O., Albinet, A., Sciare, J., and Bonsang, B.: Seasonal variability and source apportionment of volatile organic compounds (VOCs) in the Paris megacity (France), Atmos. Chem. Phys., 16, 11961-11989, https://doi.org/10.5194/acp-16-11961-2016, 2016.

Benish, S. E., He, H., Ren, X., Roberts, S. J., Salawitch, R. J., Li, Z., Wang, F., Wang, Y., Zhang, F., Shao, M., Lu, S., and Dickerson, R. R.: Measurement report: Aircraft observations of ozone, nitrogen oxides, and volatile organic compounds over Hebei Province, China, Atmos. Chem. Phys., 20, 14523-14545, https://doi.org/10.5194/acp-20-14523-2020, 2020.

Brown, S. S., Dubé, W. P., Osthoff, H. D., Stutz, J., Ryerson, T. B., Wollny, A. G., Brock, C. A., Warneke, C., de Gouw, J. A., Atlas, E., Neuman, J. A., Holloway, J. S., Lerner, B. M., Williams, E. J., Kuster, W. C., Goldan, P. D., Angevine, W. M., Trainer, M., Fehsenfeld, F. C., and Ravishankara, A. R.: Vertical profiles in NO_3 and N_2O_5 measured from an aircraft: Results from the NOAA P-3 and surface platforms during the New England Air Quality Study 2004, Journal of Geophysical Research: Atmospheres, 112, https://doi.org/10.1029/2007JD008883, 2007.

Brown, S. S., Dubé, W. P., Peischl, J., Ryerson, T. B., Atlas, E., Warneke, C., de Gouw, J. A., te Lintel Hekkert, S., Brock, C. A., Flocke, F., Trainer, M., Parrish, D. D., Feshenfeld, F. C., and Ravishankara, A. R.: Budgets for nocturnal VOC oxidation by nitrate radicals aloft during the 2006 Texas Air Quality Study, Journal of Geophysical Research: Atmospheres, 116, https://doi.org/10.1029/2011JD016544, 2011.

Caputi, D. J., Faloona, I., Trousdell, J., Smoot, J., Falk, N., and Conley, S.: Residual layer ozone, mixing, and the nocturnal jet in California's San Joaquin Valley, Atmos. Chem. Phys., 19, 4721-4740, https://doi.org/10.5194/acp-19-4721-2019, 2019.

Chen, Q., Li, X.-B., Song, R., Wang, H.-W., Li, B., He, H.-D., and Peng, Z.-R.:

Development and utilization of hexacopter unmanned aerial vehicle platform to characterize vertical distribution of boundary layer ozone in wintertime, Atmospheric Pollution Research, 11, 1073-1083, https://doi.org/10.1016/j.apr.2020.04.002, 2020.

Chen, X., Millet, D. B., Singh, H. B., Wisthaler, A., Apel, E. C., Atlas, E. L., Blake, D. R., Bourgeois, I., Brown, S. S., Crounse, J. D., de Gouw, J. A., Flocke, F. M., Fried, A., Heikes, B. G., Hornbrook, R. S., Mikoviny, T., Min, K. E., Müller, M., Neuman, J. A., O'Sullivan, D. W., Peischl, J., Pfister, G. G., Richter, D., Roberts, J. M., Ryerson, T. B., Shertz, S. R., Thompson, C. R., Treadaway, V., Veres, P. R., Walega, J., Warneke, C., Washenfelder, R. A., Weibring, P., and Yuan, B.: On the sources and sinks of atmospheric VOCs: an integrated analysis of recent aircraft campaigns over North America, Atmos. Chem. Phys., 19, 9097-9123, https://doi.org/10.5194/acp-19-9097-2019, 2019.

Coggon, M. M., Gkatzelis, G. I., McDonald, B. C., Gilman, J. B., Schwantes, R. H., Abuhassan, N., Aikin, K. C., Arend, M. F., Berkoff, T. A., Brown, S. S., Campos, T. L., Dickerson, R. R., Gronoff, G., Hurley, J. F., Isaacman-VanWertz, G., Koss, A. R., Li, M., McKeen, S. A., Moshary, F., Peischl, J., Pospisilova, V., Ren, X., Wilson, A., Wu, Y., Trainer, M., and Warneke, C.: Volatile chemical product emissions enhance ozone and modulate urban chemistry, Proceedings of the National Academy of Sciences, 118, e2026653118, https://doi.org/10.1073/pnas.2026653118, 2021.

de Gouw, J., and Warneke, C.: Measurements of volatile organic compounds in the earth's atmosphere using proton-transfer-reaction mass spectrometry, Mass Spectrom Rev, 26, 223-257, https://doi.org/10.1002/mas.20119, 2007.

de Gouw, J. A., Goldan, P. D., Warneke, C., Kuster, W. C., Roberts, J. M., Marchewka, M., Bertman, S. B., Pszenny, A. A. P., and Keene, W. C.: Validation of proton transfer reaction-mass spectrometry (PTR-MS) measurements of gas-phase organic compounds in the atmosphere during the New England Air Quality Study (NEAQS) in 2002, Journal of Geophysical Research: Atmospheres, 108, https://doi.org/10.1029/2003jd003863, 2003a.

de Gouw, J. A., Warneke, C., Parrish, D. D., Holloway, J. S., Trainer, M., and Fehsenfeld, F. C.: Emission sources and ocean uptake of acetonitrile (CH3CN) in the atmosphere, Journal of Geophysical Research: Atmospheres, 108, https://doi.org/10.1029/2002JD002897, 2003b.

de Gouw, J. A., Gilman, J. B., Kim, S.-W., Lerner, B. M., Isaacman-VanWertz, G., McDonald, B. C., Warneke, C., Kuster, W. C., Lefer, B. L., Griffith, S. M., Dusanter, S., Stevens, P. S., and Stutz, J.: Chemistry of Volatile Organic Compounds in the Los Angeles basin: Nighttime Removal of Alkenes and Determination of Emission Ratios, Journal of Geophysical Research: Atmospheres, 122, 11,843-811,861, https://doi.org/10.1002/2017JD027459, 2017.

de Gouw, J. A., Gilman, J. B., Kim, S.-W., Alvarez, S. L., Dusanter, S., Graus, M., Griffith, S. M., Isaacman-VanWertz, G., Kuster, W. C., Lefer, B. L., Lerner, B. M., McDonald, B. C., Rappenglück, B., Roberts, J. M., Stevens, P. S., Stutz, J., Thalman, R., Veres, P. R., Volkamer, R., Warneke, C., Washenfelder, R. A., and Young, C. J.:

Chemistry of Volatile Organic Compounds in the Los Angeles Basin: Formation of Oxygenated Compounds and Determination of Emission Ratios, Journal of Geophysical Research: Atmospheres, 123, 2298-2319, https://doi.org/10.1002/2017JD027976, 2018.

Deming, B. L., Pagonis, D., Liu, X., Day, D. A., Talukdar, R., Krechmer, J. E., de Gouw, J. A., Jimenez, J. L., and Ziemann, P. J.: Measurements of delays of gas-phase compounds in a wide variety of tubing materials due to gas–wall interactions, Atmos. Meas. Tech., 12, 3453-3461, 10.5194/amt-12-3453-2019, 2019.

Dieu Hien, V. T., Lin, C., Thanh, V. C., Kim Oanh, N. T., Thanh, B. X., Weng, C.-E., Yuan, C.-S., and Rene, E. R.: An overview of the development of vertical sampling technologies for ambient volatile organic compounds (VOCs), J Environ Manage, 247, 401-412, https://doi.org/10.1016/j.jenvman.2019.06.090, 2019.

Fan, M.-Y., Zhang, Y.-L., Lin, Y.-C., Li, L., Xie, F., Hu, J., Mozaffar, A., and Cao, F.: Source apportionments of atmospheric volatile organic compounds in Nanjing, China during high ozone pollution season, Chemosphere, 263, 128025, https://doi.org/10.1016/j.chemosphere.2020.128025, 2021.

Fry, J. L., Brown, S. S., Middlebrook, A. M., Edwards, P. M., Campuzano-Jost, P., Day, D. A., Jimenez, J. L., Allen, H. M., Ryerson, T. B., Pollack, I., Graus, M., Warneke, C., de Gouw, J. A., Brock, C. A., Gilman, J., Lerner, B. M., Dubé, W. P., Liao, J., and Welti, A.: Secondary organic aerosol (SOA) yields from NO_3 radical + isoprene based on nighttime aircraft power plant plume transects, Atmos. Chem. Phys., 18, 11663-11682, https://doi.org/10.5194/acp-18-11663-2018, 2018.

Geng, F., Zhang, Q., Tie, X., Huang, M., Ma, X., Deng, Z., Yu, Q., Quan, J., and Zhao, C.: Aircraft measurements of O_3, NOx, CO, VOCs, and SO_2 in the Yangtze River Delta region, Atmos Environ, 43, 584-593, https://doi.org/10.1016/j.atmosenv.2008.10.021, 2009.

Geyer, A., and Stutz, J.: Vertical profiles of NO_3, N_2O_5, O_3, and NOx in the nocturnal boundary layer: 2. Model studies on the altitude dependence of composition and chemistry, Journal of Geophysical Research: Atmospheres, 109, https://doi.org/10.1029/2003jd004211, 2004.

Gkatzelis, G. I., Coggon, M. M., McDonald, B. C., Peischl, J., Gilman, J. B., Aikin, K. C., Robinson, M. A., Canonaco, F., Prevot, A. S. H., Trainer, M., and Warneke, C.: Observations Confirm that Volatile Chemical Products Are a Major Source of Petrochemical Emissions in U.S. Cities, Environ Sci Technol, https://doi.org/10.1021/acs.est.0c05471, 2021.

Gómez, M. C., Durana, N., García, J. A., de Blas, M., Sáez de Cámara, E., García-Ruiz, E., Gangoiti, G., Torre-Pascual, E., and Iza, J.: Long-term measurement of biogenic volatile organic compounds in a rural background area: Contribution to ozone formation, Atmos Environ, 224, 117315, https://doi.org/10.1016/j.atmosenv.2020.117315, 2020.

Greenberg, J. P., Guenther, A., Zimmerman, P., Baugh, W., Geron, C., Davis, K., Helmig, D., and Klinger, L. F.: Tethered balloon measurements of biogenic VOCs in

the atmospheric boundary layer, Atmos Environ, 33, 855-867, https://doi.org/10.1016/S1352-2310(98)00302-1, 1999.

Guo, H., Cheng, H. R., Ling, Z. H., Louie, P. K. K., and Ayoko, G. A.: Which emission sources are responsible for the volatile organic compounds in the atmosphere of Pearl River Delta?, J Hazard Mater, 188, 116-124, https://doi.org/10.1016/j.jhazmat.2011.01.081, 2011.

Hayes, P. L., Ortega, A. M., Cubison, M. J., Froyd, K. D., Zhao, Y., Cliff, S. S., Hu, W. W., Toohey, D. W., Flynn, J. H., Lefer, B. L., Grossberg, N., Alvarez, S., Rappenglück, B., Taylor, J. W., Allan, J. D., Holloway, J. S., Gilman, J. B., Kuster, W. C., de Gouw, J. A., Massoli, P., Zhang, X., Liu, J., Weber, R. J., Corrigan, A. L., Russell, L. M., Isaacman, G., Worton, D. R., Kreisberg, N. M., Goldstein, A. H., Thalman, R., Waxman, E. M., Volkamer, R., Lin, Y. H., Surratt, J. D., Kleindienst, T. E., Offenberg, J. H., Dusanter, S., Griffith, S., Stevens, P. S., Brioude, J., Angevine, W. M., and Jimenez, J. L.: Organic aerosol composition and sources in Pasadena, California, during the 2010 CalNex campaign, Journal of Geophysical Research: Atmospheres, 118, 9233-9257, https://doi.org/10.1002/jgrd.50530, 2013.

He, X., Yuan, B., Wu, C., Wang, S., Wang, C., Huangfu, Y., Qi, J., Ma, N., Xu, W., Wang, M., Chen, W., Su, H., Cheng, Y., and Shao, M.: Volatile organic compounds in wintertime North China Plain: Insights from measurements of proton transfer reaction time-of-flight mass spectrometer (PTR-ToF-MS), Journal of Environmental Sciences, https://doi.org/10.1016/j.jes.2021.08.010, 2022.

Hornbrook, R. S., Blake, D. R., Diskin, G. S., Fried, A., Fuelberg, H. E., Meinardi, S., Mikoviny, T., Richter, D., Sachse, G. W., Vay, S. A., Walega, J., Weibring, P., Weinheimer, A. J., Wiedinmyer, C., Wisthaler, A., Hills, A., Riemer, D. D., and Apel, E. C.: Observations of nonmethane organic compounds during ARCTAS − Part 1: Biomass burning emissions and plume enhancements, Atmos. Chem. Phys., 11, 11103-11130, 10.5194/acp-11-11103-2011, 2011.

Hu, L., Millet, D. B., Mohr, M. J., Wells, K. C., Griffis, T. J., and Helmig, D.: Sources and seasonality of atmospheric methanol based on tall tower measurements in the US Upper Midwest, Atmos. Chem. Phys., 11, 11145-11156, https://doi.org/10.5194/acp-11-11145-2011, 2011.

Hu, L., Millet, D. B., Kim, S. Y., Wells, K. C., Griffis, T. J., Fischer, E. V., Helmig, D., Hueber, J., and Curtis, A. J.: North American acetone sources determined from tall tower measurements and inverse modeling, Atmos. Chem. Phys., 13, 3379-3392, https://doi.org/10.5194/acp-13-3379-2013, 2013.

Hu, L., Millet, D. B., Baasandorj, M., Griffis, T. J., Travis, K. R., Tessum, C. W., Marshall, J. D., Reinhart, W. F., Mikoviny, T., Müller, M., Wisthaler, A., Graus, M., Warneke, C., and de Gouw, J.: Emissions of C6–C8 aromatic compounds in the United States: Constraints from tall tower and aircraft measurements, Journal of Geophysical Research: Atmospheres, 120, 826-842, https://doi.org/10.1002/2014JD022627, 2015a.

Hu, L., Millet, D. B., Baasandorj, M., Griffis, T. J., Turner, P., Helmig, D., Curtis, A. J., and Hueber, J.: Isoprene emissions and impacts over an ecological transition

844 region in the U.S. Upper Midwest inferred from tall tower measurements, Journal of
845 Geophysical Research: Atmospheres, 120, 3553-3571,
846 https://doi.org/10.1002/2014jd022732, 2015b.

847 Hu, W., Hu, M., Hu, W., Jimenez, J. L., Yuan, B., Chen, W., Wang, M., Wu, Y.,
848 Chen, C., Wang, Z., Peng, J., Zeng, L., and Shao, M.: Chemical composition, sources,
849 and aging process of submicron aerosols in Beijing: Contrast between summer and
850 winter, Journal of Geophysical Research: Atmospheres, 121, 1955-1977,
851 https://doi.org/10.1002/2015JD024020, 2016.

852 Huang, X., Ding, A., Gao, J., Zheng, B., Zhou, D., Qi, X., Tang, R., Wang, J., Ren,
853 C., Nie, W., Chi, X., Xu, Z., Chen, L., Li, Y., Che, F., Pang, N., Wang, H., Tong, D.,
854 Qin, W., Cheng, W., Liu, W., Fu, Q., Liu, B., Chai, F., Davis, S. J., Zhang, Q., and He,
855 K.: Enhanced secondary pollution offset reduction of primary emissions during
856 COVID-19 lockdown in China, National Science Review, 8,
857 https://doi.org/10.1093/nsr/nwaa137, 2020.

858 Huangfu, Y., Yuan, B., Wang, S., Wu, C., He, X., Qi, J., de Gouw, J., Warneke, C.,
859 Gilman, J. B., Wisthaler, A., Karl, T., Graus, M., Jobson, B. T., and Shao, M.: Revisiting
860 Acetonitrile as Tracer of Biomass Burning in Anthropogenic-Influenced Environments,
861 Geophys Res Lett, 48, e2020GL092322, https://doi.org/10.1029/2020GL092322, 2021.

862 Jin, X., Li, Z., Wu, T., Wang, Y., Cheng, Y., Su, T., Wei, J., Ren, R., Wu, H., Li, S.,
863 Zhang, D., and Cribb, M.: The different sensitivities of aerosol optical properties to
864 particle concentration, humidity, and hygroscopicity between the surface level and the
865 upper boundary layer in Guangzhou, China, Sci Total Environ, 803, 150010,
866 https://doi.org/10.1016/j.scitotenv.2021.150010, 2022.

867 Klein, F., Farren, N. J., Bozzetti, C., Daellenbach, K. R., Kilic, D., Kumar, N. K.,
868 Pieber, S. M., Slowik, J. G., Tuthill, R. N., Hamilton, J. F., Baltensperger, U., Prévôt,
869 A. S. H., and El Haddad, I.: Indoor terpene emissions from cooking with herbs and
870 pepper and their secondary organic aerosol production potential, Scientific Reports, 6,
871 36623, 10.1038/srep36623, 2016.

872 Koss, A., Yuan, B., Warneke, C., Gilman, J. B., Lerner, B. M., Veres, P. R., Peischl,
873 J., Eilerman, S., Wild, R., Brown, S. S., Thompson, C. R., Ryerson, T., Hanisco, T.,
874 Wolfe, G. M., Clair, J. M. S., Thayer, M., Keutsch, F. N., Murphy, S., and de Gouw, J.:
875 Observations of VOC emissions and photochemical products over US oil- and gas-
876 producing regions using high-resolution H_3O^+ CIMS (PTR-ToF-MS), Atmospheric
877 Measurement Techniques, 10, http://dx.doi.org/10.5194/amt-10-2941-2017, 2017.

878 Li, X.-B., Wang, D., Lu, Q.-C., Peng, Z.-R., Fu, Q., Hu, X.-M., Huo, J., Xiu, G.,
879 Li, B., Li, C., Wang, D.-S., and Wang, H.: Three-dimensional analysis of ozone and
880 $PM_{2.5}$ distributions obtained by observations of tethered balloon and unmanned aerial
881 vehicle in Shanghai, China, Stoch Env Res Risk A, 32, 1189-1203,
882 https://doi.org/10.1007/s00477-018-1524-2, 2018.

883 Li, X.-B., Fan, G., Lou, S., Yuan, B., Wang, X., and Shao, M.: Transport and
884 boundary layer interaction contribution to extremely high surface ozone levels in
885 eastern China, Environ Pollut, 268, 115804,

886 https://doi.org/10.1016/j.envpol.2020.115804, 2021a.

887 Li, X.-B., Peng, Z.-R., Wang, D., Li, B., Huangfu, Y., Fan, G., Wang, H., and Lou,
888 S.: Vertical distributions of boundary-layer ozone and fine aerosol particles during the
889 emission control period of the G20 summit in Shanghai, China, Atmospheric Pollution
890 Research, 12, 352-364, https://doi.org/10.1016/j.apr.2020.09.016, 2021b.

891 Li, X.-B., Yuan, B., Parrish, D. D., Chen, D., Song, Y., Yang, S., Liu, Z., and Shao,
892 M.: Long-term trend of ozone in southern China reveals future mitigation strategy for
893 air pollution, Atmos Environ, 269, 118869, 10.1016/j.atmosenv.2021.118869, 2022.

894 Liebmann, J., Sobanski, N., Schuladen, J., Karu, E., Hellén, H., Hakola, H., Zha,
895 Q., Ehn, M., Riva, M., Heikkinen, L., Williams, J., Fischer, H., Lelieveld, J., and
896 Crowley, J. N.: Alkyl nitrates in the boreal forest: formation via the NO_3^-, OH^- and O_3-
897 induced oxidation of biogenic volatile organic compounds and ambient lifetimes,
898 Atmos. Chem. Phys., 19, 10391-10403, https://doi.org/10.5194/acp-19-10391-2019,
899 2019.

900 Liu, B., Liang, D., Yang, J., Dai, Q., Bi, X., Feng, Y., Yuan, J., Xiao, Z., Zhang, Y.,
901 and Xu, H.: Characterization and source apportionment of volatile organic compounds
902 based on 1-year of observational data in Tianjin, China, Environ Pollut, 218, 757-769,
903 https://doi.org/10.1016/j.envpol.2016.07.072, 2016.

904 Liu, X., Deming, B., Pagonis, D., Day, D. A., Palm, B. B., Talukdar, R., Roberts,
905 J. M., Veres, P. R., Krechmer, J. E., Thornton, J. A., de Gouw, J. A., Ziemann, P. J., and
906 Jimenez, J. L.: Effects of gas–wall interactions on measurements of semivolatile
907 compounds and small polar molecules, Atmos. Meas. Tech., 12, 3137-3149,
908 10.5194/amt-12-3137-2019, 2019.

909 Liu, Y., Wang, H., Jing, S., Zhou, M., Lou, S., Qu, K., Qiu, W., Wang, Q., Li, S.,
910 Gao, Y., Liu, Y., Li, X., Peng, Z.-R., Chen, J., and Lu, K.: Vertical Profiles of Volatile
911 Organic Compounds in Suburban Shanghai, Adv Atmos Sci, 38, 1177-1187,
912 https://doi.org/10.1007/s00376-021-0126-y, 2021.

913 Ma, Z., Zhang, X., Xu, J., Zhao, X., and Meng, W.: Characteristics of ozone
914 vertical profile observed in the boundary layer around Beijing in autumn, Journal of
915 Environmental Sciences, 23, 1316-1324, https://doi.org/10.1016/s1001-
916 0742(10)60557-8, 2011.

917 McDonald, B. C., de Gouw, J. A., Gilman, J. B., Jathar, S. H., Akherati, A., Cappa,
918 C. D., Jimenez, J. L., Lee-Taylor, J., Hayes, P. L., McKeen, S. A., Cui, Y. Y., Kim, S.-
919 W., Gentner, D. R., Isaacman-VanWertz, G., Goldstein, A. H., Harley, R. A., Frost, G.
920 J., Roberts, J. M., Ryerson, T. B., and Trainer, M.: Volatile chemical products emerging
921 as largest petrochemical source of urban organic emissions, Science, 359, 760,
922 https://doi.org/10.1126/science.aaq0524, 2018.

923 Millet, D. B., Apel, E., Henze, D. K., Hill, J., Marshall, J. D., Singh, H. B., and
924 Tessum, C. W.: Natural and Anthropogenic Ethanol Sources in North America and
925 Potential Atmospheric Impacts of Ethanol Fuel Use, Environ Sci Technol, 46, 8484-
926 8492, https://doi.org/10.1021/es300162u, 2012.

927 Millet, D. B., Baasandorj, M., Hu, L., Mitroo, D., Turner, J., and Williams, B. J.:

Nighttime Chemistry and Morning Isoprene Can Drive Urban Ozone Downwind of a Major Deciduous Forest, Environ Sci Technol, 50, 4335-4342, https://doi.org/10.1021/acs.est.5b06367, 2016.

Mo, Z., Shao, M., and Lu, S.: Compilation of a source profile database for hydrocarbon and OVOC emissions in China, Atmos Environ, 143, 209-217, https://doi.org/10.1016/j.atmosenv.2016.08.025, 2016.

Mo, Z., Huang, S., Yuan, B., Pei, C., Song, Q., Qi, J., Wang, M., Wang, B., Wang, C., Li, M., Zhang, Q., and Shao, M.: Deriving emission fluxes of volatile organic compounds from tower observation in the Pearl River Delta, China, Sci Total Environ, 741, 139763, https://doi.org/10.1016/j.scitotenv.2020.139763, 2020.

Müller, M., Anderson, B. E., Beyersdorf, A. J., Crawford, J. H., Diskin, G. S., Eichler, P., Fried, A., Keutsch, F. N., Mikoviny, T., Thornhill, K. L., Walega, J. G., Weinheimer, A. J., Yang, M., Yokelson, R. J., and Wisthaler, A.: In situ measurements and modeling of reactive trace gases in a small biomass burning plume, Atmos. Chem. Phys., 16, 3813-3824, 10.5194/acp-16-3813-2016, 2016.

Ng, N. L., Brown, S. S., Archibald, A. T., Atlas, E., Cohen, R. C., Crowley, J. N., Day, D. A., Donahue, N. M., Fry, J. L., Fuchs, H., Griffin, R. J., Guzman, M. I., Herrmann, H., Hodzic, A., Iinuma, Y., Jimenez, J. L., Kiendler-Scharr, A., Lee, B. H., Luecken, D. J., Mao, J. Q., McLaren, R., Mutzel, A., Osthoff, H. D., Ouyang, B., Picquet-Varrault, B., Platt, U., Pye, H. O. T., Rudich, Y., Schwantes, R. H., Shiraiwa, M., Stutz, J., Thornton, J. A., Tilgner, A., Williams, B. J., and Zaveri, R. A.: Nitrate radicals and biogenic volatile organic compounds: oxidation, mechanisms, and organic aerosol, Atmos. Chem. Phys., 17, 2103-2162, https://doi.org/10.5194/acp-17-2103-2017, 2017.

Pallavi, Sinha, B., and Sinha, V.: Source apportionment of volatile organic compounds in the northwest Indo-Gangetic Plain using a positive matrix factorization model, Atmos. Chem. Phys., 19, 15467-15482, https://doi.org/10.5194/acp-19-15467-2019, 2019.

Pernov, J. B., Bossi, R., Lebourgeois, T., Nøjgaard, J. K., Holzinger, R., Hjorth, J. L., and Skov, H.: Atmospheric VOC measurements at a High Arctic site: characteristics and source apportionment, Atmos. Chem. Phys., 21, 2895-2916, https://doi.org/10.5194/acp-21-2895-2021, 2021.

Qi, J., Mo, Z., Yuan, B., Huang, S., Huangfu, Y., Wang, Z., Li, X., Yang, S., Wang, W., Zhao, Y., Wang, X., Wang, W., Liu, K., and Shao, M.: An observation approach in evaluation of ozone production to precursor changes during the COVID-19 lockdown, Atmos Environ, 262, 118618, https://doi.org/10.1016/j.atmosenv.2021.118618, 2021.

Qin, J., Wang, X., Yang, Y., Qin, Y., Shi, S., Xu, P., Chen, R., Zhou, X., Tan, J., and Wang, X.: Source apportionment of VOCs in a typical medium-sized city in North China Plain and implications on control policy, Journal of Environmental Sciences, 107, 26-37, https://doi.org/10.1016/j.jes.2020.10.005, 2021.

Sangiorgi, G., Ferrero, L., Perrone, M. G., Bolzacchini, E., Duane, M., and Larsen, B. R.: Vertical distribution of hydrocarbons in the low troposphere below and above the

mixing height: Tethered balloon measurements in Milan, Italy, Environ Pollut, 159, 3545-3552, https://doi.org/10.1016/j.envpol.2011.08.012, 2011.

Squires, F. A., Nemitz, E., Langford, B., Wild, O., Drysdale, W. S., Acton, W. J. F., Fu, P., Grimmond, C. S. B., Hamilton, J. F., Hewitt, C. N., Hollaway, M., Kotthaus, S., Lee, J., Metzger, S., Pingintha-Durden, N., Shaw, M., Vaughan, A. R., Wang, X., Wu, R., Zhang, Q., and Zhang, Y.: Measurements of traffic-dominated pollutant emissions in a Chinese megacity, Atmos. Chem. Phys., 20, 8737-8761, https://doi.org/10.5194/acp-20-8737-2020, 2020.

Stutz, J., Alicke, B., Ackermann, R., Geyer, A., White, A., and Williams, E.: Vertical profiles of NO_3, N_2O_5, O_3, and NO_x in the nocturnal boundary layer: 1. Observations during the Texas Air Quality Study 2000, Journal of Geophysical Research: Atmospheres, 109, https://doi.org/10.1029/2003jd004209, 2004.

Tan, Y., Han, S., Chen, Y., Zhang, Z., Li, H., Li, W., Yuan, Q., Li, X., Wang, T., and Lee, S.-c.: Characteristics and source apportionment of volatile organic compounds (VOCs) at a coastal site in Hong Kong, Sci Total Environ, 777, 146241, https://doi.org/10.1016/j.scitotenv.2021.146241, 2021.

Ting, M., Yue-si, W., Jie, J., Fang-kun, W., and Mingxing, W.: The vertical distributions of VOCs in the atmosphere of Beijing in autumn, Sci Total Environ, 390, 97-108, https://doi.org/10.1016/j.scitotenv.2007.08.035, 2008.

Udina, M., Soler, M. R., Olid, M., Jiménez-Esteve, B., and Bech, J.: Pollutant vertical mixing in the nocturnal boundary layer enhanced by density currents and low-level jets: two representative case studies, Bound-lay Meteorol, 174, 203-230, https://doi.org/10.1007/s10546-019-00483-y, 2020.

Ulbrich, I. M., Canagaratna, M. R., Zhang, Q., Worsnop, D. R., and Jimenez, J. L.: Interpretation of organic components from Positive Matrix Factorization of aerosol mass spectrometric data, Atmos. Chem. Phys., 9, 2891-2918, https://doi.org/10.5194/acp-9-2891-2009, 2009.

Velasco, E., Marquez, C., Bueno, E., Bernabe, R. M., Sanchez, A., Fentanes, O., Wohrnschimmel, H., Cardenas, B., Kamilla, A., Wakamatsu, S., and Molina, L. T.: Vertical distribution of ozone and VOCs in the low boundary layer of Mexico City, Atmos. Chem. Phys., 8, 3061-3079, https://doi.org/10.5194/acp-8-3061-2008, 2008.

Veres, P. R., Faber, P., Drewnick, F., Lelieveld, J., and Williams, J.: Anthropogenic sources of VOC in a football stadium: Assessing human emissions in the atmosphere, Atmos Environ, 77, 1052-1059, https://doi.org/10.1016/j.atmosenv.2013.05.076, 2013.

Vo, T.-D.-H., Lin, C., Weng, C.-E., Yuan, C.-S., Lee, C.-W., Hung, C.-H., Bui, X.-T., Lo, K.-C., and Lin, J.-X.: Vertical stratification of volatile organic compounds and their photochemical product formation potential in an industrial urban area, J Environ Manage, 217, 327-336, https://doi.org/10.1016/j.jenvman.2018.03.101, 2018.

Wang, C., Yuan, B., Wu, C., Wang, S., Qi, J., Wang, B., Wang, Z., Hu, W., Chen, W., Ye, C., Wang, W., Sun, Y., Wang, C., Huang, S., Song, W., Wang, X., Yang, S., Zhang, S., Xu, W., Ma, N., Zhang, Z., Jiang, B., Su, H., Cheng, Y., Wang, X., and Shao, M.: Measurements of higher alkanes using NO+ chemical ionization in PTR-ToF-MS:

1012 important contributions of higher alkanes to secondary organic aerosols in China,
1013 Atmos. Chem. Phys., 20, 14123-14138, https://doi.org/10.5194/acp-20-14123-2020,
1014 2020a.

1015 Wang, T., Xue, L., Brimblecombe, P., Lam, Y. F., Li, L., and Zhang, L.: Ozone
1016 pollution in China: A review of concentrations, meteorological influences, chemical
1017 precursors, and effects, Sci Total Environ, 575, 1582-1596,
1018 https://doi.org/10.1016/j.scitotenv.2016.10.081, 2017.

1019 Wang, Y., Wang, Y., Tang, G., Yang, Y., Li, X., Yao, D., Wu, S., Kang, Y., Wang,
1020 M., and Wang, Y.: High gaseous carbonyl concentrations in the upper boundary layer
1021 in Shijiazhuang, China, Sci Total Environ, 799, 149438,
1022 https://doi.org/10.1016/j.scitotenv.2021.149438, 2021.

1023 Wang, Y. H., Gao, W. K., Wang, S., Song, T., Gong, Z. Y., Ji, D. S., Wang, L. L.,
1024 Liu, Z. R., Tang, G. Q., Huo, Y. F., Tian, S. L., Li, J. Y., Li, M. G., Yang, Y., Chu, B. W.,
1025 Petaja, T., Kerminen, V. M., He, H., Hao, J. M., Kulmala, M., Wang, Y. S., and Zhang,
1026 Y. H.: Contrasting trends of PM$_{2.5}$ and surface-ozone concentrations in China from 2013
1027 to 2017, National Science Review, 7, 1331-1339, https://doi.org/10.1093/nsr/nwaa032,
1028 2020b.

1029 Wang, Z., Yuan, B., Ye, C., Roberts, J., Wisthaler, A., Lin, Y., Li, T., Wu, C., Peng,
1030 Y., Wang, C., Wang, S., Yang, S., Wang, B., Qi, J., Wang, C., Song, W., Hu, W., Wang,
1031 X., Xu, W., Ma, N., Kuang, Y., Tao, J., Zhang, Z., Su, H., Cheng, Y., Wang, X., and
1032 Shao, M.: High Concentrations of Atmospheric Isocyanic Acid (HNCO) Produced from
1033 Secondary Sources in China, Environ Sci Technol, 54, 11818-11826,
1034 https://doi.org/10.1021/acs.est.0c02843, 2020c.

1035 Warneke, C., de Gouw, J. A., Goldan, P. D., Kuster, W. C., Williams, E. J., Lerner,
1036 B. M., Jakoubek, R., Brown, S. S., Stark, H., Aldener, M., Ravishankara, A. R., Roberts,
1037 J. M., Marchewka, M., Bertman, S., Sueper, D. T., McKeen, S. A., Meagher, J. F., and
1038 Fehsenfeld, F. C.: Comparison of daytime and nighttime oxidation of biogenic and
1039 anthropogenic VOCs along the New England coast in summer during New England Air
1040 Quality Study 2002, Journal of Geophysical Research: Atmospheres, 109,
1041 https://doi.org/10.1029/2003jd004424, 2004.

1042 Wu, C., Wang, C., Wang, S., Wang, W., Yuan, B., Qi, J., Wang, B., Wang, H., Wang,
1043 C., Song, W., Wang, X., Hu, W., Lou, S., Ye, C., Peng, Y., Wang, Z., Huangfu, Y., Xie,
1044 Y., Zhu, M., Zheng, J., Wang, X., Jiang, B., Zhang, Z., and Shao, M.: Measurement
1045 report: Important contributions of oxygenated compounds to emissions and chemistry
1046 of volatile organic compounds in urban air, Atmos. Chem. Phys., 20, 14769-14785,
1047 https://doi.org/10.5194/acp-20-14769-2020, 2020a.

1048 Wu, F., Yu, Y., Sun, J., Zhang, J., Wang, J., Tang, G., and Wang, Y.: Characteristics,
1049 source apportionment and reactivity of ambient volatile organic compounds at Dinghu
1050 Mountain in Guangdong Province, China, Sci Total Environ, 548-549, 347-359,
1051 https://doi.org/10.1016/j.scitotenv.2015.11.069, 2016.

1052 Wu, S., Tang, G., Wang, Y., Yang, Y., Yao, D., Zhao, W., Gao, W., Sun, J., and
1053 Wang, Y.: Vertically decreased VOC concentration and reactivity in the planetary

boundary layer in winter over the North China Plain, Atmos Res, 240, 104930, https://doi.org/10.1016/j.atmosres.2020.104930, 2020b.

Wu, S., Tang, G. Q., Wang, Y. H., Mai, R., Yao, D., Kang, Y. Y., Wang, Q. L., and Wang, Y. S.: Vertical Evolution of Boundary Layer Volatile Organic Compounds in Summer over the North China Plain and the Differences with Winter, Adv Atmos Sci, 38, 1165-1176, https://doi.org/10.1007/s00376-020-0254-9, 2021.

Xia, S.-Y., Wang, C., Zhu, B., Chen, X., Feng, N., Yu, G.-H., and Huang, X.-F.: Long-term observations of oxygenated volatile organic compounds (OVOCs) in an urban atmosphere in southern China, 2014–2019, Environ Pollut, 270, 116301, https://doi.org/10.1016/j.envpol.2020.116301, 2021.

Xue, L., Wang, T., Simpson, I. J., Ding, A., Gao, J., Blake, D. R., Wang, X., Wang, W., Lei, H., and Jin, D.: Vertical distributions of non-methane hydrocarbons and halocarbons in the lower troposphere over northeast China, Atmos Environ, 45, 6501-6509, https://doi.org/10.1016/j.atmosenv.2011.08.072, 2011.

Yan, F., Chen, W., Jia, S., Zhong, B., Yang, L., Mao, J., Chang, M., Shao, M., Yuan, B., Situ, S., Wang, X., Chen, D., and Wang, X.: Stabilization for the secondary species contribution to PM$_{2.5}$ in the Pearl River Delta (PRD) over the past decade, China: A meta-analysis, Atmos Environ, 242, 117817, https://doi.org/10.1016/j.atmosenv.2020.117817, 2020.

Ye, C., Yuan, B., Lin, Y., Wang, Z., Hu, W., Li, T., Chen, W., Wu, C., Wang, C., Huang, S., Qi, J., Wang, B., Wang, C., Song, W., Wang, X., Zheng, E., Krechmer, J. E., Ye, P., Zhang, Z., Wang, X., Worsnop, D. R., and Shao, M.: Chemical characterization of oxygenated organic compounds in the gas phase and particle phase using iodide CIMS with FIGAERO in urban air, Atmos. Chem. Phys., 21, 8455-8478, https://doi.org/10.5194/acp-21-8455-2021, 2021.

Yuan, B., Shao, M., de Gouw, J., Parrish, D. D., Lu, S., Wang, M., Zeng, L., Zhang, Q., Song, Y., Zhang, J., and Hu, M.: Volatile organic compounds (VOCs) in urban air: How chemistry affects the interpretation of positive matrix factorization (PMF) analysis, Journal of Geophysical Research: Atmospheres, 117, https://doi.org/10.1029/2012jd018236, 2012.

Yuan, B., Koss, A., Warneke, C., Gilman, J. B., Lerner, B. M., Stark, H., and de Gouw, J. A.: A high-resolution time-of-flight chemical ionization mass spectrometer utilizing hydronium ions (H$_3$O+ ToF-CIMS) for measurements of volatile organic compounds in the atmosphere, Atmospheric Measurement Techniques, 9, 2735-2752, https://doi.org/10.5194/amt-9-2735-2016, 2016.

Yuan, B., Koss, A. R., Warneke, C., Coggon, M., Sekimoto, K., and de Gouw, J. A.: Proton-Transfer-Reaction Mass Spectrometry: Applications in Atmospheric Sciences, Chem Rev, 117, 13187-13229, https://doi.org/10.1021/acs.chemrev.7b00325, 2017.

Yuan, Z., Zhong, L., Lau, A. K. H., Yu, J. Z., and Louie, P. K. K.: Volatile organic compounds in the Pearl River Delta: Identification of source regions and recommendations for emission-oriented monitoring strategies, Atmos Environ, 76, 162-

172, https://doi.org/10.1016/j.atmosenv.2012.11.034, 2013.

Zhang, H., Zhang, Y., Huang, Z., Acton, W. J. F., Wang, Z., Nemitz, E., Langford, B., Mullinger, N., Davison, B., Shi, Z., Liu, D., Song, W., Yang, W., Zeng, J., Wu, Z., Fu, P., Zhang, Q., and Wang, X.: Vertical profiles of biogenic volatile organic compounds as observed online at a tower in Beijing, J Environ Sci (China), 95, 33-42, https://doi.org/10.1016/j.jes.2020.03.032, 2020.

Zhang, K., Xiu, G., Zhou, L., Bian, Q., Duan, Y., Fei, D., Wang, D., and Fu, Q.: Vertical distribution of volatile organic compounds within the lower troposphere in late spring of Shanghai, Atmos Environ, 186, 150-157, https://doi.org/10.1016/j.atmosenv.2018.03.044, 2018.

Zhang, K., Zhou, L., Fu, Q., Yan, L., Bian, Q., Wang, D., and Xiu, G.: Vertical distribution of ozone over Shanghai during late spring: A balloon-borne observation, Atmos Environ, 208, 48-60, https://doi.org/10.1016/j.atmosenv.2019.03.011, 2019.

Zhang, Y., Wang, X., Barletta, B., Simpson, I. J., Blake, D. R., Fu, X., Zhang, Z., He, Q., Liu, T., Zhao, X., and Ding, X.: Source attributions of hazardous aromatic hydrocarbons in urban, suburban and rural areas in the Pearl River Delta (PRD) region, J Hazard Mater, 250-251, 403-411, https://doi.org/10.1016/j.jhazmat.2013.02.023, 2013.

Zhao, D., Pullinen, I., Fuchs, H., Schrade, S., Wu, R., Acir, I. H., Tillmann, R., Rohrer, F., Wildt, J., Guo, Y., Kiendler-Scharr, A., Wahner, A., Kang, S., Vereecken, L., and Mentel, T. F.: Highly oxygenated organic molecule (HOM) formation in the isoprene oxidation by NO_3 radical, Atmos. Chem. Phys., 21, 9681-9704, https://doi.org/10.5194/acp-21-9681-2021, 2021.

Zheng, J., Yu, Y., Mo, Z., Zhang, Z., Wang, X., Yin, S., Peng, K., Yang, Y., Feng, X., and Cai, H.: Industrial sector-based volatile organic compound (VOC) source profiles measured in manufacturing facilities in the Pearl River Delta, China, Sci Total Environ, 456-457, 127-136, https://doi.org/10.1016/j.scitotenv.2013.03.055, 2013.

Zhou, X., Li, Z., Zhang, T., Wang, F., Wang, F., Tao, Y., Zhang, X., Wang, F., and Huang, J.: Volatile organic compounds in a typical petrochemical industrialized valley city of northwest China based on high-resolution PTR-MS measurements: Characterization, sources and chemical effects, Sci Total Environ, 671, 883-896, https://doi.org/10.1016/j.scitotenv.2019.03.283, 2019.

Zhu, B., Han, Y., Wang, C., Huang, X., Xia, S., Niu, Y., Yin, Z., and He, L.: Understanding primary and secondary sources of ambient oxygenated volatile organic compounds in Shenzhen utilizing photochemical age-based parameterization method, Journal of Environmental Sciences, 75, 105-114, https://doi.org/10.1016/j.jes.2018.03.008, 2019.
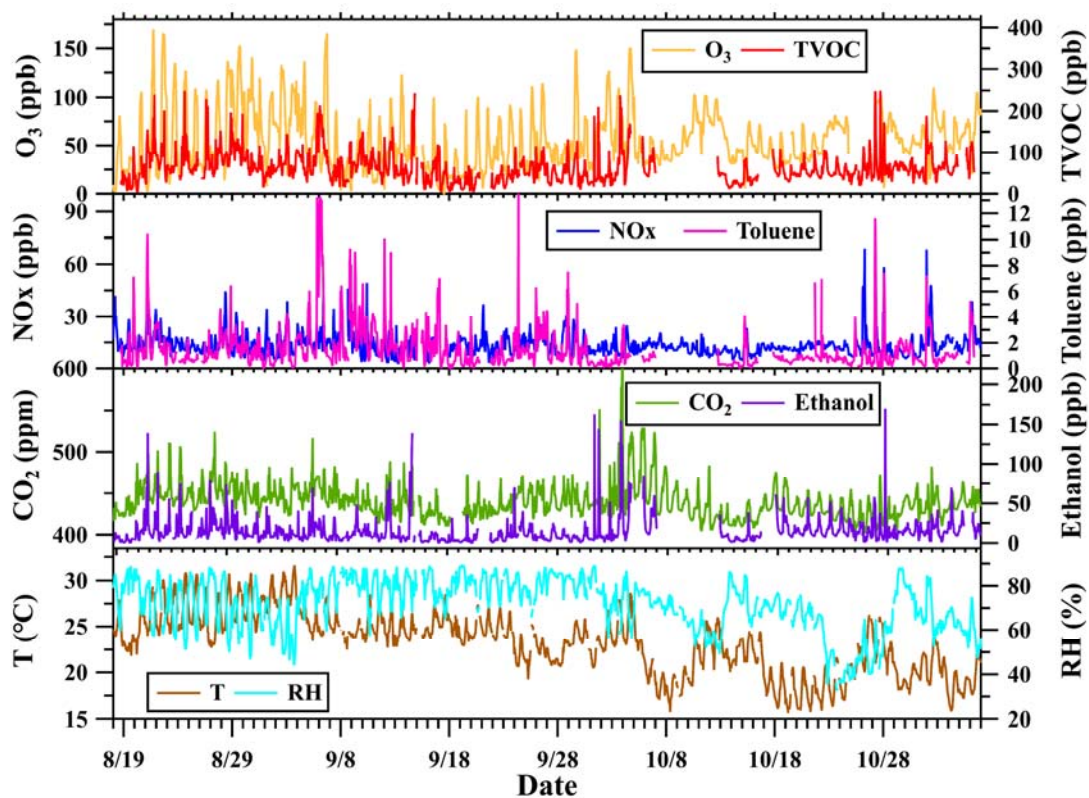
Figure 1. Time series of concentrations of some typical chemical species along with meteorological parameters (hourly averages) during the CTT campaign. Temperature (T), relative humidity (RH), concentrations of ozone and NOx were measured at 488 m. Concentrations of VOCs, ethanol, and CO_2 were measured at 450 m.
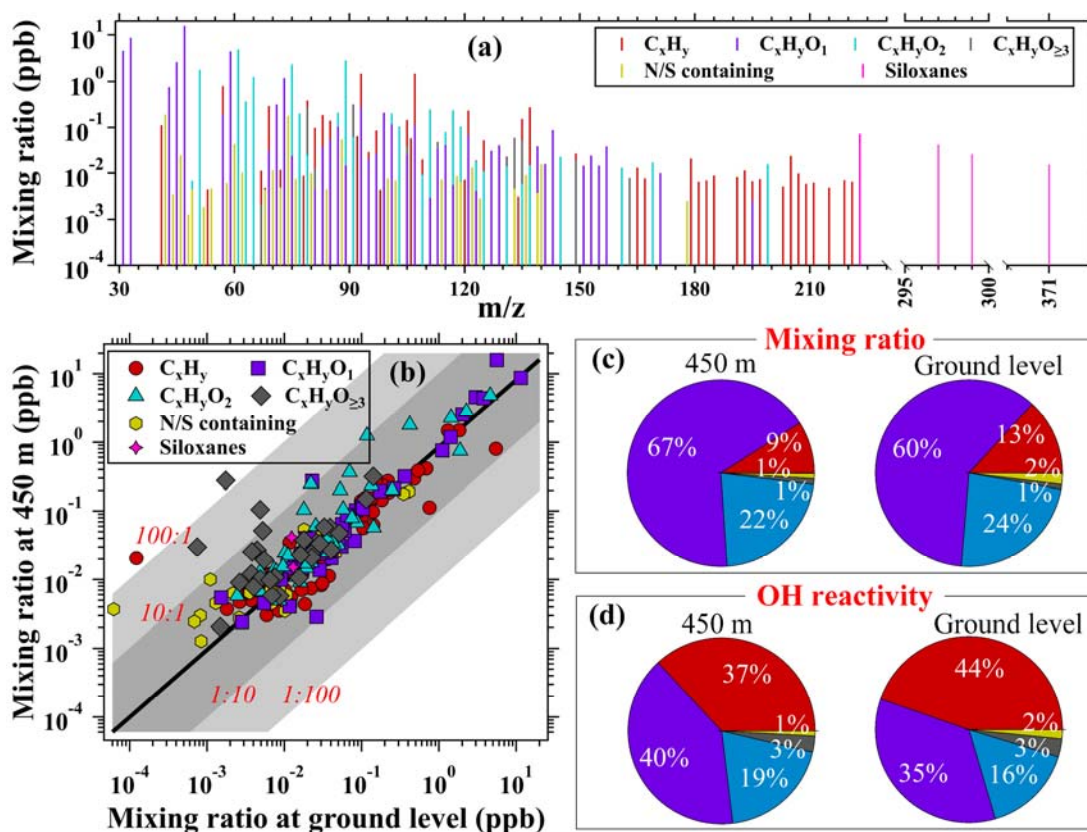
Figure 2. (a) Average mass spectra of VOCs (including 225 species) obtained by PTR-ToF-MS measured at 450 m during the CTT campaign. (b) Scatter plots of the average VOC mixing ratios measured at 450 m during the CTT campaign versus those measured at ground level during the GIG campaign; The black solid line indicates the ratio of 1:1; The dark grey shaded areas indicate the ratios of 10:1 and 1:10; The light grey shaded areas indicate the ratios of 100:1 and 1:100. (c-d) Average contribution percentages of the six VOCs categories to their total concentrations and OH reactivities at 450 m and the ground level, respectively; Only the VOCs species that have known reaction rate constants with OH radical (Table S1) were used for calculation.
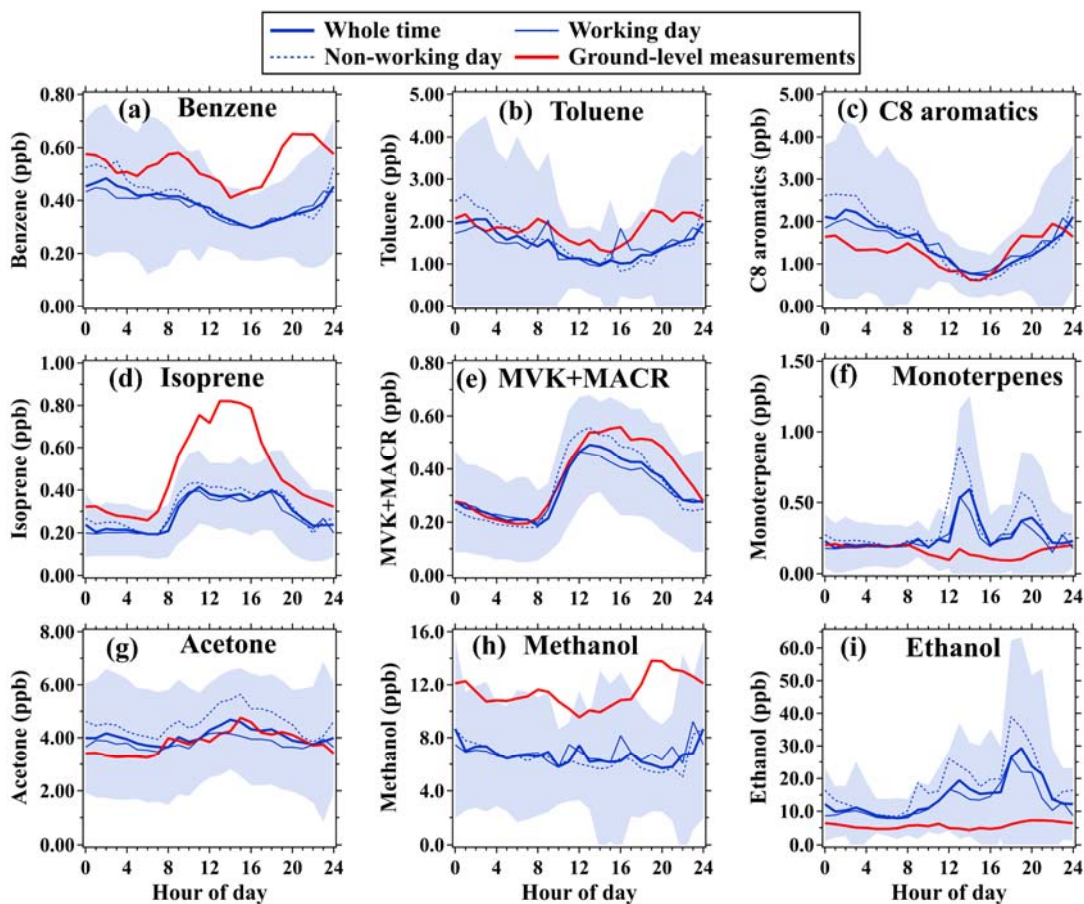
1149

1150 **Figure 3.** Diurnal variations in mixing ratios of selected VOC species measured by

1151 PTR-ToF-MS. Thick blue solid lines and shaded areas represent averages and standard

1152 deviations, respectively, during the CTT campaign (August 18–November 05, 2020).

1153 Red solid lines represent averages during the GIG campaign (September 11–November

1154 19, 2018). Thin blue solid and dashed lines represent averages in working days and

1155 non-working (including weekends and public holidays) days, respectively, during the

1156 CTT campaign.
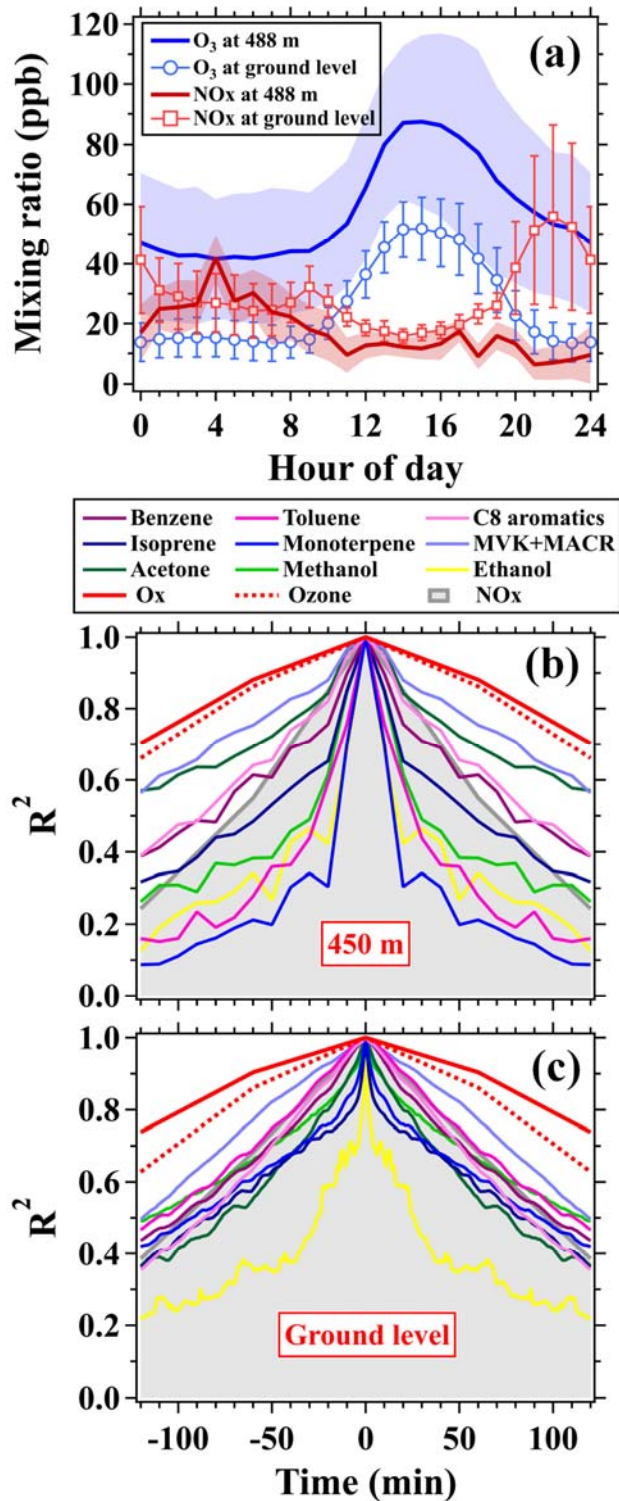
1157

Figure 4. (a) Diurnal profiles of ozone and NOx mixing ratios measured at the 488-m

site (mean ± standard deviation) and the surface site (mean ± 0.5 standard deviation)

on the CTT. (b) Autocorrelation of the time series of ozone (488 m), NOx (488 m), Ox

(488 m), and selected VOC species (450 m) during the CTT campaign. (c)

Autocorrelation of the time series of the selected VOC species at ground level during

1163   the GIG campaign; Autocorrelation of the time series of ozone, NOx, and Ox in panel

1164   (c) are calculated using the measurements made at the surface site of Canton Tower

1165   during the CTT campaign.
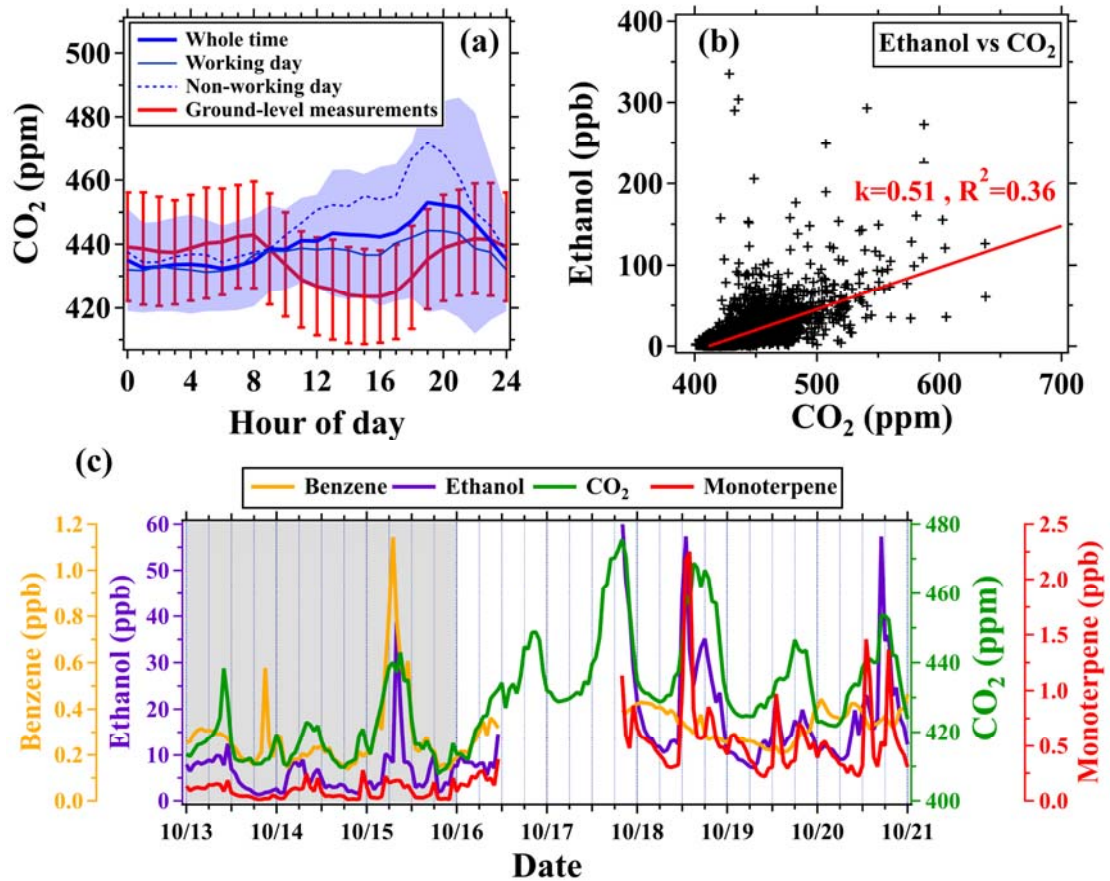
1166

Figure 5. (a) Diurnal variations in CO_2 mixing ratios at 450 m and the ground level,
respectively. (b) Scatterplots of 10-min mean mixing ratios of ethanol versus CO_2
measured at 450 m during the CTT campaign.(c) Time series of benzene, ethanol, CO_2,
and monoterpene mixing ratios measured at 450 m from October 13 to 21; The grey
shaded area indicates the period (October 13–21) when the 450-m platform was closed
due to the influence of Typhoon Kompasu.
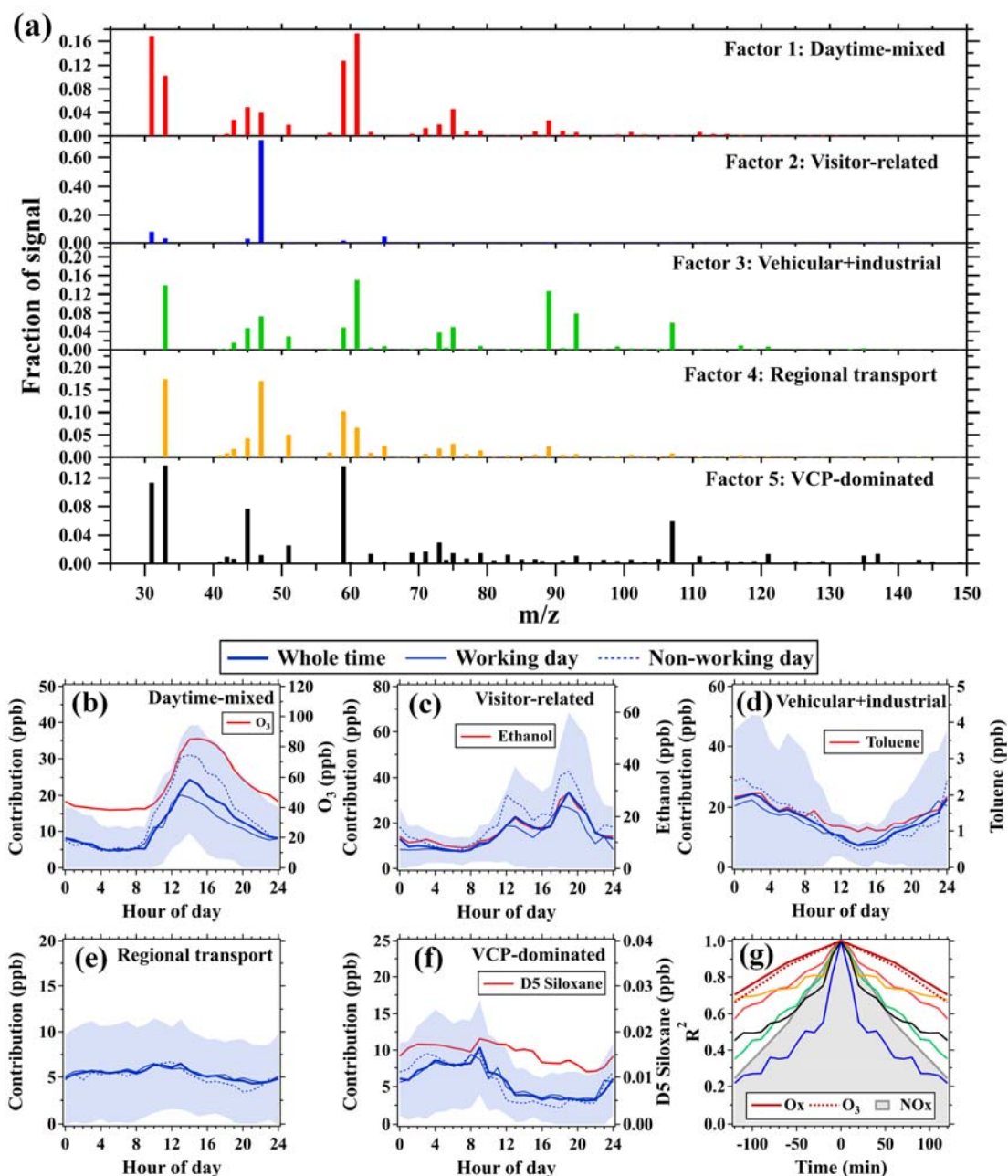
1173

1174 **Figure 6.** (a) Factor profiles (m/z ≤ 150) of the five PMF factors; Factor profiles with

1175 a full range of the mass spectra are provided in Figure S7. (b-f) Average diurnal profiles

1176 of the five PMF factors and source tracers. (g) Autocorrelation of the time series of the

1177 five PMF factors along with Ox, ozone, and NOx mixing ratios at 488 m; Colors of

1178 lines are consistent with the five factors in panel (a).
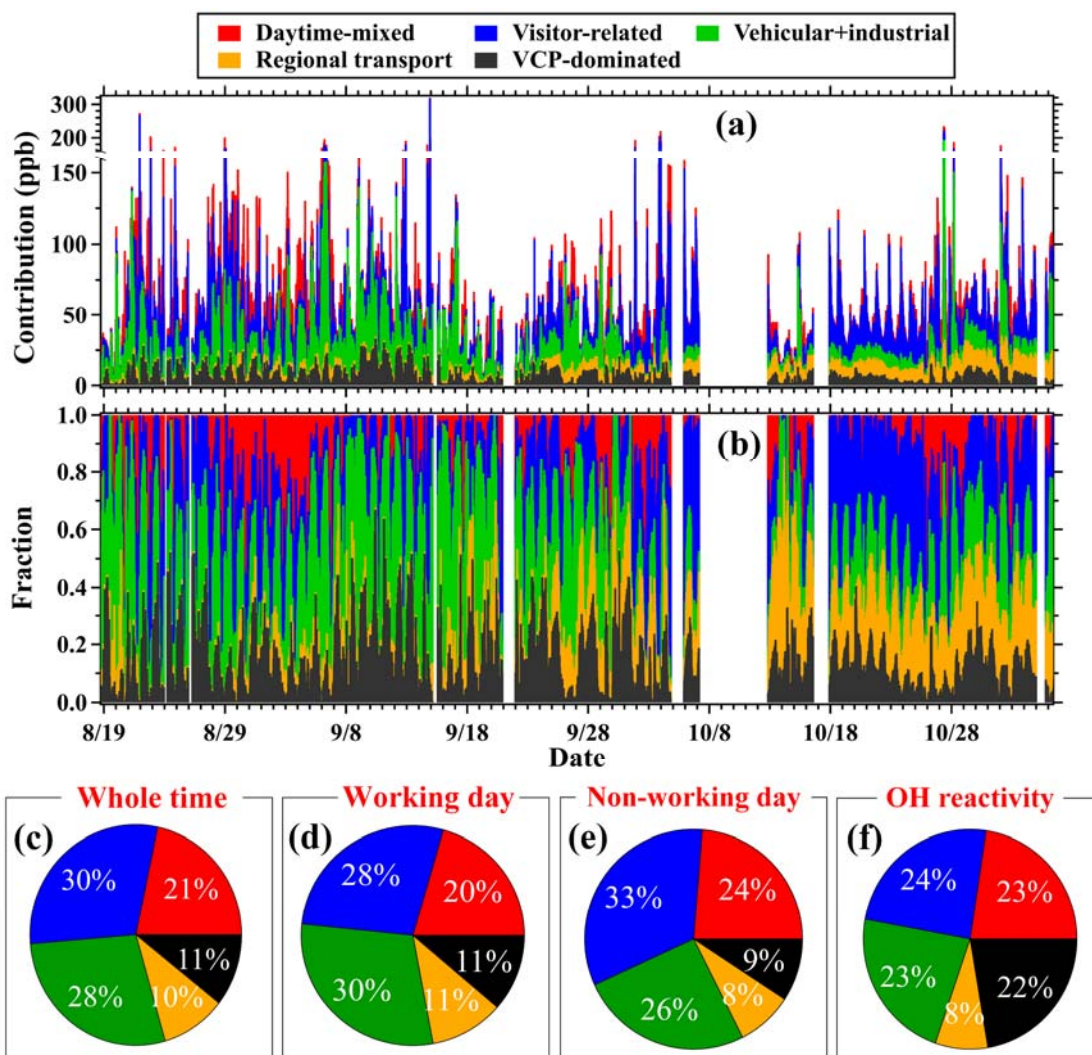
Figure 7. (a-b) Stacked time series of factor fractions and factor contributions for the PMF analysis. (c-e) Average contribution percentages of the five PMF factors to (c-e) the total VOCs concentrations in the whole time, working days, and non-working days and (f) the total OH reactivities during the CTT campaign. In panel (d), only the VOCs species that have known reaction rate constants with OH radical (Table S1) were used.
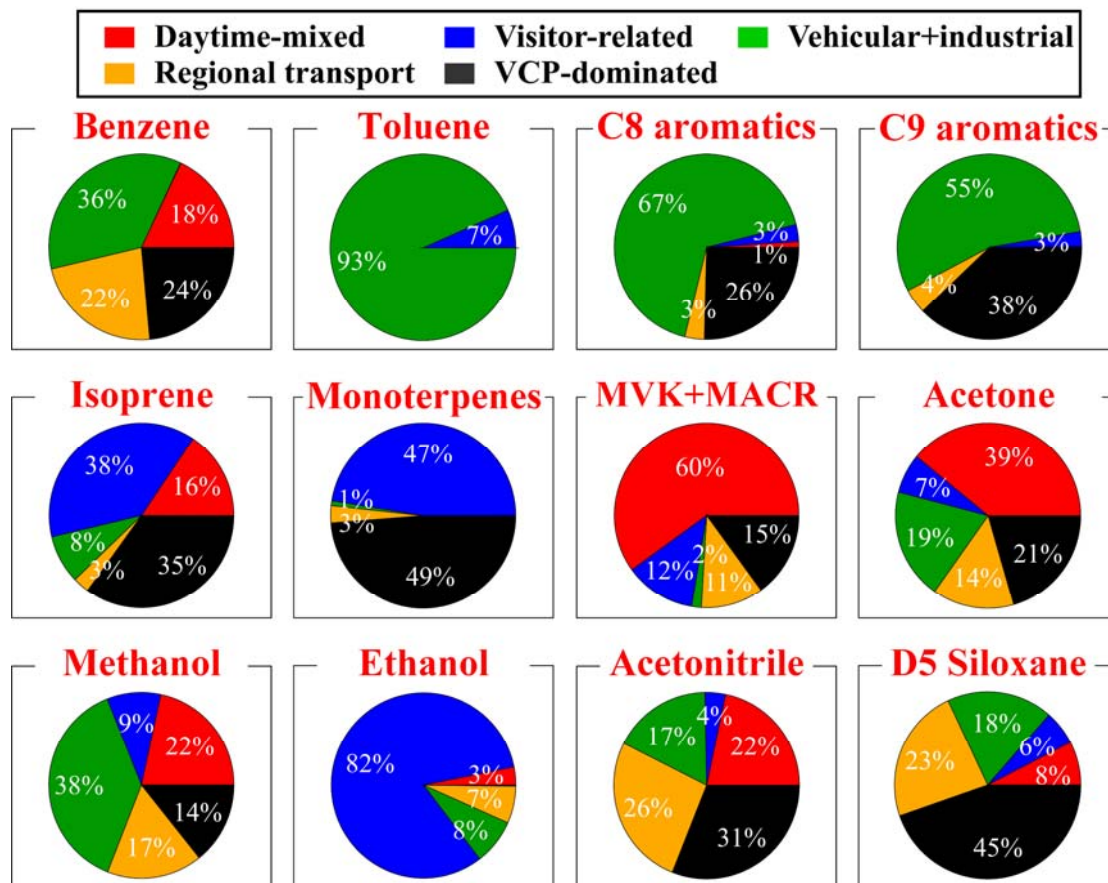
Figure 8. (a) Average contribution percentages of the five PMF factors to concentrations of the 9 selected VOC species during the CTT campaign.
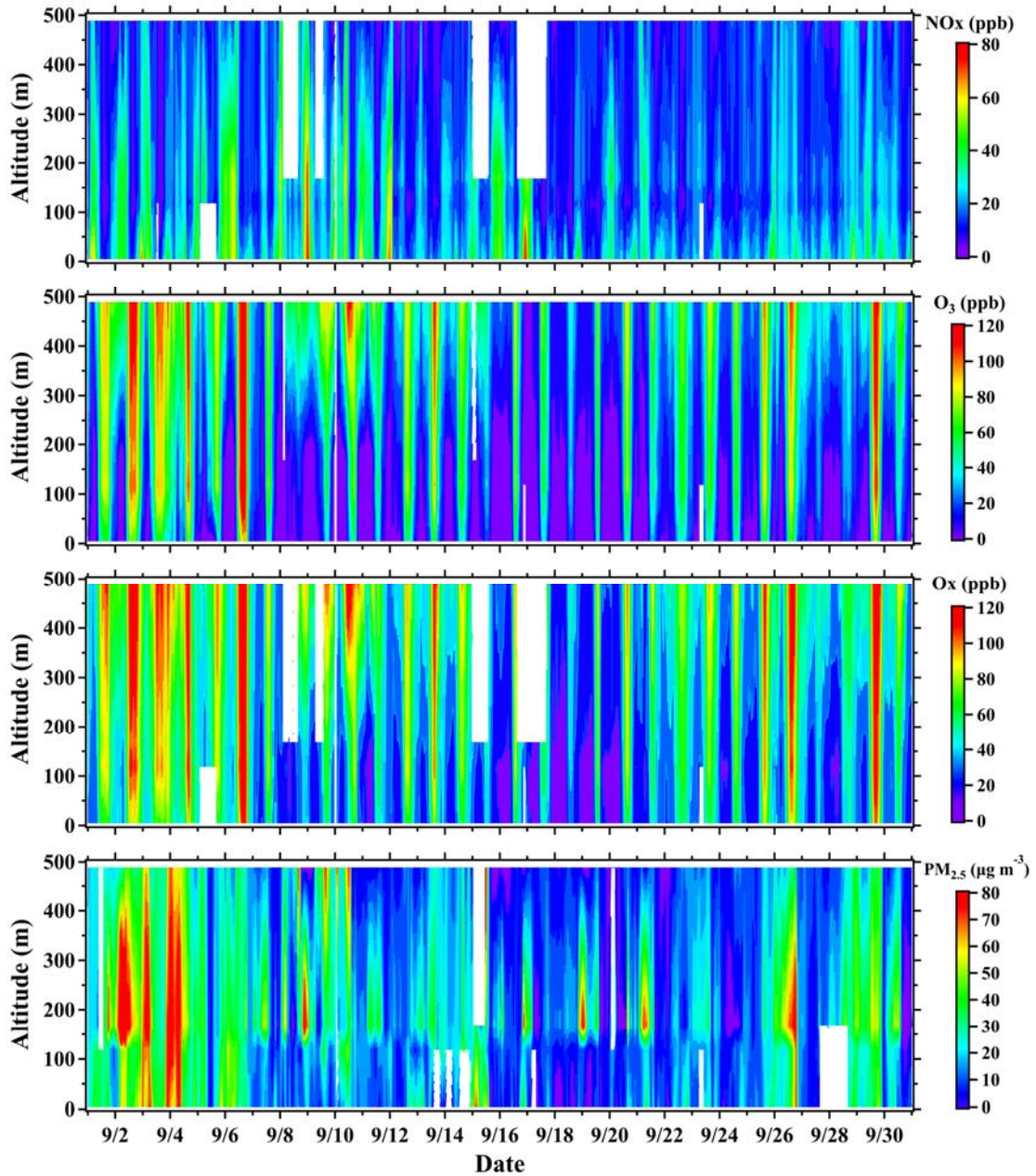
Figure 9. Time series of vertical profiles for O_3, NOx, Ox (O_3+NO_2), and $PM_{2.5}$ concentrations in September during the CTT campaign. The contour plots are made using the measurements from the four CTT sites (5 m, 118 m, 168 m, and 488 m).
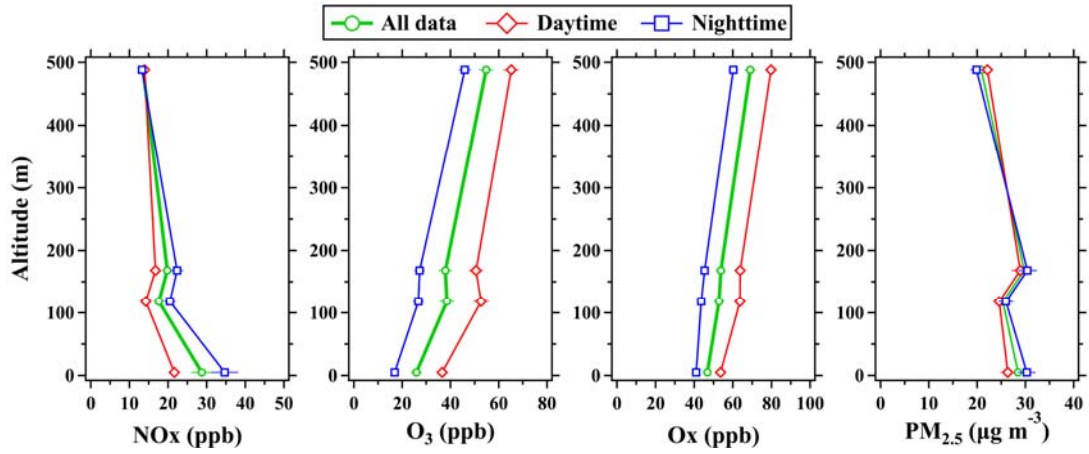
1192

Figure 10. Average vertical profiles of O_3, NOx, Ox (O_3+NO_2), and PM$_{2.5}$ concentrations (mean ± 0.1 standard deviations) measured at the four CTT sites (5 m, 118 m, 168 m, 488 m) during the campaign. Daytime refers to the time between LT 08:00–18:00; nighttime refers to the time between LT 19:00–05:00.
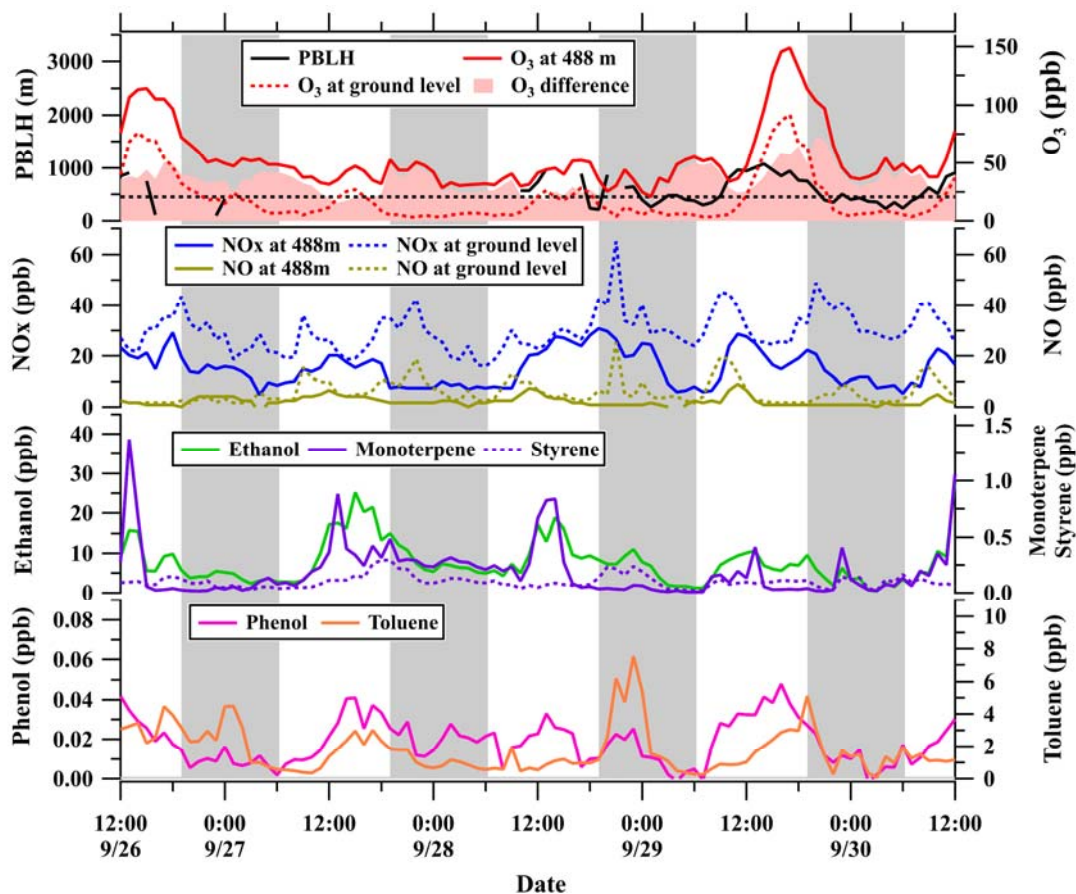
Figure 11. Time series of O_3, NOx, NO, ethanol, monoterpene, styrene, phenol, and toluene mixing ratios along with planetary boundary layer height (PBLH) during September 26–30. O_3 difference refers to the differences in ozone mixing ratios between 488 m and 5 m. Grey shaded areas indicate nighttime periods (LT 19:00–05:00).